J. Fluid Mech. (2015), *vol.* 768, *pp.* 51–90.
doi:10.1017/jfm.2015.48

Mixed convection in a periodically heated channel

M. Z. Hossain[1,†] **and J. M. Floryan**[1]

[1]Department of Mechanical and Materials Engineering, The University of Western Ontario, London, Ontario, ON N6A 5B9, Canada

(Received 27 June 2014; revised 13 October 2014; accepted 21 January 2015; first published online 3 March 2015)

Mixed convection in a channel with flow driven by a pressure gradient and subject to spatially periodic heating along one of the walls has been studied. The pattern of the heating is characterized by the wavenumber α and its intensity is expressed in terms of the Rayleigh number Ra_p. The primary convection has the form of counter-rotating rolls with the wavevector parallel to the wavevector of the heating. The resulting net heat flow between the walls increases proportionally to Ra_p but the growth saturates when $Ra_p = O(10^3)$. The most effective heating pattern corresponds to $\alpha \approx 1$, as this leads to the most intense transverse motion. The primary convection is subject to transition to secondary states with the onset conditions depending on α. The conditions leading to transition between different forms of secondary motion have been determined using the linear stability theory. Three patterns of secondary motion may occur at small Reynolds numbers Re, i.e. longitudinal rolls, transverse rolls and oblique rolls, with the critical conditions varying significantly as a function of α. An increase of α leads to the elimination of the longitudinal rolls and, eventually, to the elimination of the oblique rolls, with the transverse rolls assuming the dominant role. For large α, the transition is driven by the Rayleigh–Bénard mechanism; while for $\alpha = O(1)$, the spatial parametric resonance dominates. The global flow characteristics are identical regardless of whether the heating is applied at the lower or the upper wall.

Key words: buoyancy-driven instability, convection

1. Introduction

There are numerous heat transfer systems where the heat flow is driven by spatially distributed heating. Efficient heat removal from components installed on computer motherboards represents one typical situation. Natural convection is preferred due to its passive character but it can rarely handle the required heat load. Weather phenomena associated with non-uniform heating of the ground represent another example. This effect is related to the presence of patterns of roofs–streets–parks in an urban environment and forests–lakes–fields in a rural environment. The use of flow patterning for biological applications such as cell analysers provides an interesting application in microfluidics (Krishnan, Ugaz & Burns 2002). Understanding of the

† Email address for correspondence: mhossa7@uwo.ca

motions of fluids over geometrically, chemically and thermally patterned surfaces is of vital interest in their design. Of particular importance is how convective motions develop and how they affect the transport of passive scalar quantities along regularly structured surfaces (Beltrame *et al.* 2011). It is known in geological applications that a system of fractures, leads and polynyas in sea ice leads to convection in both the ocean and the atmosphere, with small leads of the order of several metres being more efficient than larger ones of the order of several hundred metres (Marcq & Weiss 2012). The insulating effect of continents on mantle convection within the Earth is another example of a spatially structured convection occurring in nature (Lenardic *et al.* 2005).

The heat transport in the case of pure natural convection is driven by the buoyancy force. Convection occurring in a stationary fluid layer subject to spatially homogeneous heating from below represents the reference case. This is the so-called Rayleigh–Bénard (RB) convection (Bénard 1900; Rayleigh 1916). The conductive state of equilibrium undergoes transition to convective motion if the critical conditions expressed in terms of a suitably defined Rayleigh number are met; see Bodenschatz, Pesch & Ahlers (2000), Ahlers, Grossmann & Lohse (2009), Lohse & Xia (2010) and Chilla & Schumacher (2012) for recent reviews. The RB convection can be combined with inhomogeneities in the boundary temperatures, but this concept has been used only to study the effects of small inhomogeneities (or boundary imperfections) on the symmetry breakup in the RB convection rather than to investigate convection dominated by such inhomogeneities (Hossain & Floryan 2013*b*). The introduction of forced motion (mixed convection) gives preference to rolls with axes parallel to the flow direction but does not affect the critical conditions (Gage & Reid 1968); see Kelly (1994) for a complete review.

Inhomogeneous heating creates horizontal temperature variations, which lead to different vertical pressure distributions at different horizontal locations, giving rise to horizontal pressure gradients. Such configurations are statically unstable, resulting in fluid movement regardless of the intensity of the heating and leading to motion frequently referred to as horizontal convection (Maxworthy 1997; Siggers, Kerswell & Balmforth 2004; Hughes & Griffiths 2008; Winters & Young 2009). The first study of such convection that we are aware of used asymptotic approximation in the analysis of long-wavelength heating (Kelly & Pal 1976*a*,*b*). A detailed analysis of convection resulting from application of heating with arbitrary wavelength and with arbitrary Prandtl number has been given only recently (Hossain & Floryan 2013*a*). It has been shown that the heat transfer strongly depends on the wavenumber; it rapidly decreases when the wavenumber is either too small or too large. The primary convection undergoes transition to secondary convection whose structure strongly depends on the heating wavenumber (Hossain & Floryan 2013*b*). For large wavenumbers, the primary convection creates a conduction zone above a thin boundary layer adjacent to the heated wall, resulting in the dominance of the RB mechanism. When heating wavenumbers are $O(1)$, the spatial parametric resonance dominates, resulting in the formation of oblique rolls with the wavevector having a component orthogonal to the wavevector of the primary convection. Such oblique structures are rarely observed in pattern-forming systems, where they lead to the three-dimensionalization of the otherwise two-dimensional flow problem. It has been shown that wavenumber locking between the primary and secondary convection occurs under certain conditions. A qualitatively similar problem with spatial variability resulting from the use of mixed insulating and conducting boundary conditions has been studied by Ripesi *et al.* (2014) using numerical simulations.

In many applications, spatially distributed heating is combined with forced motion. It has been shown recently that spatially periodic heating gives rise to the superthermohydrophobic effect (Floryan 2012; Hossain, Floryan & Floryan 2012), which leads to a significant drag reduction for small Re flows and thus could lead to the design of a new class of microfluidic devices. These predictions remain valid as long as the flow does not undergo transition to secondary states. The first study of secondary states that we are aware of is due to Hasnaoui *et al.* (1991), who used two-dimensional direct numerical simulations and observed a number of complex secondary states. Their analysis cannot capture oblique rolls as well as rolls with axes parallel to the flow direction, which play the dominant role in mixed convection with uniform heating (Gage & Reid 1968; Kelly 1994). It can be concluded that the characteristics of mixed convection in a system subject to spatially periodic heating are not known. The conditions leading to transition to secondary states as well as flow patterns resulting from such transition remain to be determined.

The main objective of this analysis is to determine the basic characteristics of fluid movement and the resulting heat transfer process associated with mixed convection in a simple system consisting of an infinitely long horizontal channel where the flow is driven by a pressure gradient and the channel is subject to heating that is periodic in the flow direction. We shall focus our attention on fluids with $Pr = 0.71$ and consider a simple sinusoidal temperature variation applied at the lower wall, as this reduces the number of parameters to just three, i.e. the heating wavenumber α, the heating intensity expressed in terms of the Rayleigh number Ra_p, and the flow Reynolds number Re. The convective motion resulting from the applied heating can be viewed as a forced response or, alternatively, it can be referred to as the primary convection. It is known that convective flows are highly unstable, and thus the analysis is extended to include determination of conditions leading to secondary convection as well as determination of the possible patterns of secondary motions. The analysis is carried out using a model problem where the heating is applied at the lower wall. Generalization of the results to the heating applied at the upper wall is discussed, as the system exhibits up–down symmetries (Howard & Krishnamurti 1986; Hossain & Floryan 2014).

The rest of this paper is organized as follows. Section 2 discusses the forced response of the fluid, i.e. the primary convection. Section 3 discusses transition to secondary states as well as flow topologies associated with these states using linear stability theory as the main methodology. Section 4 provides a summary of the main conclusions.

2. Primary convection

The external heating of interest is a function of the streamwise coordinate and it results in a two-dimensional steady primary convection. The three-dimensional secondary convection is discussed in § 3.

2.1. *Problem formulation with heating applied at the lower wall*

Consider fluid contained in a slot between two parallel plates extending to $\pm\infty$ in the x and z directions and placed at a distance $2h$ apart from each other, with the gravitational acceleration g acting in the negative y direction, as shown in figure 1. The fluid is driven in the positive x direction by a constant pressure gradient, resulting in a two-dimensional motion. The upper plate is kept isothermal with the constant

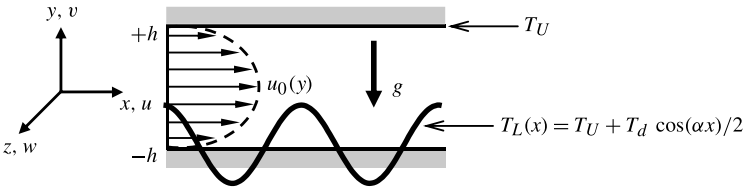

FIGURE 1. Sketch of the flow system.

temperature T_U, while the lower plate is subject to periodic heating resulting in its temperature T_L of the form

$$T_L(x) = T_U + \tfrac{1}{2} T_d \cos(\alpha x), \tag{2.1}$$

where $\lambda = 2\pi/\alpha$ is the wavelength of the heating. The fluid is incompressible and Newtonian, with thermal conductivity k, specific heat c, thermal diffusivity $\kappa = k/\rho c$, kinematic viscosity ν, dynamic viscosity μ, thermal expansion coefficient Γ and variations of the density ρ that follow the Boussinesq approximation. All material properties are taken at the reference temperature T_U.

The dimensionless form of the velocity and pressure fields in the absence of the heating are expressed as

$$\boldsymbol{v}_0(x, y) = [u_0(y), 0] = [1 - y^2, 0], \quad p_0(x, y) = -2x/Re, \tag{2.2a,b}$$

where $\boldsymbol{v}_0$ denotes the velocity vector scaled with the maximum of the x velocity U_{max}, p_0 stands for the pressure scaled with ρU_{max}^2, half of the distance between the plates h has been chosen as the length scale and the Reynolds number is defined as $Re = U_{max} h/\nu$.

Introduction of the heating modifies the above fields, which can be represented as a superposition of the pressure-gradient-driven and the buoyancy-driven motions. The temperature field can be represented, for convenience of interpretation, as a superposition of the conductive field θ_0 corresponding to the external heating and modifications associated with the movement of the fluid. Here $\theta_0 = (T - T_U)$ stands for the relative temperature. The complete flow quantities are identified using the subscript B and have the form

$$\left.\begin{aligned} u_B(x, y) = Re\, u_0(y) + u_1(x, y), \quad v_B(x, y) = v_1(x, y), \\ \theta_B(x, y) = Pr^{-1}\theta_0(x, y) + \theta_1(x, y), \quad p_B(x, y) = Re^2 p_0(x) + p_1(x, y), \end{aligned}\right\} \tag{2.3}$$

where (u_1, v_1), p_1 and θ_1 stand for the part of the velocity vector, the pressure and the temperature associated with the buoyancy effects. The complete velocity vector (u_B, v_B) and the velocity modifications (u_1, v_1) have been scaled using the convective velocity scale $U_v = \nu/h$, where $U_{max}/U_v = Re$, the complete pressure field p_B as well as the pressure modifications p_1 have been scaled using ρU_v^2, the complete temperature field θ_B as well as the temperature modifications θ_1 have been scaled with the convective temperature scale $T_v = T_d \nu/\kappa$, while the conductive temperature field has been scaled with T_d as the relevant scale, where $T_v/T_d = Pr$ and Pr stands for the Prandtl number. The reader may note that the maximum of θ_B in this scaling is always $(2Pr)^{-1}$. The conductive temperature field is described by the system

$$\nabla^2\theta_0 = 0, \quad \theta_0(+1) = 0, \quad \theta_0(-1) = \tfrac{1}{2}\cos(\alpha x), \tag{2.4a–c}$$

where ∇^2 denotes the Laplace operator. Its solution has the form

$$\theta_0(x, y) = \frac{1}{4}\left[-\frac{\sinh(\alpha y)}{\sinh(\alpha)} + \frac{\cosh(\alpha y)}{\cosh(\alpha)}\right]\cos(\alpha x) = \theta_0^{(1)}(y)\mathrm{e}^{\mathrm{i}\alpha x} + \theta_0^{(-1)}(y)\mathrm{e}^{-\mathrm{i}\alpha x}, \tag{2.5}$$

and demonstrates that conductive effects do not generate net heat flow across the channel. The dimensionless field equations for the flow and temperature modifications take the form

$$(Re\, u_0 + u_1)\frac{\partial u_1}{\partial x} + Re\, v_1\frac{\mathrm{d}u_0}{\mathrm{d}y} + v_1\frac{\partial u_1}{\partial y} = -\frac{\partial p_1}{\partial x} + \nabla^2 u_1, \tag{2.6a}$$

$$(Re\, u_0 + u_1)\frac{\partial v_1}{\partial x} + v_1\frac{\partial v_1}{\partial y} = -\frac{\partial p_1}{\partial y} + \nabla^2 v_1 + Ra_p\theta_1 + Ra_p Pr^{-1}\theta_0, \tag{2.6b}$$

$$Pr\left((Re\, u_0 + u_1)\frac{\partial \theta_1}{\partial x} + v_1\frac{\partial \theta_1}{\partial y}\right) + (Re\, u_0 + u_1)\frac{\partial \theta_0}{\partial x} + v_1\frac{\partial \theta_0}{\partial y} = \nabla^2\theta_1, \tag{2.6c}$$

$$\frac{\partial u_1}{\partial x} + \frac{\partial v_1}{\partial y} = 0, \tag{2.6d}$$

where $Ra_p = g\Gamma h^3 T_d/\nu\kappa$ is the Rayleigh number that measures the intensity of the heating. Our main interest is in the determination of the aperiodic part of the temperature modification θ_1, as it provides information about the net heat flow. The presence of convection affects the drag experienced by the fluid, which, in turn, may lead to a different flow rate and thus may affect the convective heat transfer. The formulation is finalized by imposing the fixed flow-rate constraint, i.e. the flow rate must be the same in the isothermal as well as in the heated channels. The explicit form of this constraint can be written as

$$Q = \int_{-1}^{1} u_B\,\mathrm{d}y = \int_{-1}^{1}(Re\, u_0 + u_1)\,\mathrm{d}y = 4\,Re/3. \tag{2.7}$$

The relevant boundary conditions include the no-slip and the no-penetration conditions as well as the thermal boundary of the form

$$u_1(\pm 1) = 0, \quad v_1(\pm 1) = 0, \quad \theta_1(\pm 1) = 0. \tag{2.8a–c}$$

Solution of (2.6)–(2.8) results in the simultaneous determination of the velocity and temperature fields, followed by determination of the heat flow characteristics. The limit of $Re \to 0$ corresponds to a pure natural convection studied by Hossain & Floryan (2013*a*,*b*). An increase of Re leads to an increase in the importance of the forced flow. Elimination of the heating corresponds to the limit $Ra_p \to 0$, which results in $u_1 = v_1 = p_1 = \theta_1 = 0$ with the flow field being described by (2.2*a*,*b*).

2.2. *Numerical solution method*

The numerical algorithm used in this analysis is similar to that employed by Hossain & Floryan (2013*b*) and thus the following presentation is limited to a short outline. Introduction of the stream function $\psi(x, y)$, defined in the usual manner, i.e. $u_1 = \partial\psi/\partial y$, $v_1 = -\partial\psi/\partial x$, and elimination of pressure brings the governing equations to the form

$$Re\, u_0\frac{\partial}{\partial x}(\nabla^2\psi) - Re\frac{\mathrm{d}^2 u_0}{\mathrm{d}y^2}\frac{\partial\psi}{\partial x} + N_\psi = \nabla^4\psi - Ra_p\frac{\partial\theta_1}{\partial x} - Ra_p Pr^{-1}\frac{\partial\theta_0}{\partial x}, \tag{2.9a}$$

$$PrRe\,u_0\frac{\partial\theta_1}{\partial x}+Pr\,N_{\theta1}+Re\,u_0\frac{\partial\theta_0}{\partial x}+N_{\theta0}=\nabla^2\theta_1, \tag{2.9b}$$

where ∇^4 denotes the biharmonic operator, the nonlinear terms are written in the conservative form, i.e.

$$N_\psi=\frac{\partial}{\partial y}\left(\frac{\partial}{\partial x}\langle u_1u_1\rangle+\frac{\partial}{\partial y}\langle u_1v_1\rangle\right)-\frac{\partial}{\partial x}\left(\frac{\partial}{\partial x}\langle u_1v_1\rangle+\frac{\partial}{\partial y}\langle v_1v_1\rangle\right), \tag{2.10}$$

$$N_{\theta1}=\frac{\partial}{\partial x}\langle u_1\theta_1\rangle+\frac{\partial}{\partial y}\langle v_1\theta_1\rangle,\quad N_{\theta0}=\frac{\partial}{\partial x}\langle u_1\theta_0\rangle+\frac{\partial}{\partial y}\langle v_1\theta_0\rangle \tag{2.11a,b}$$

and $\langle\cdots\rangle$ denotes products. The solution is assumed to be in the form of Fourier expansions

$$\psi(x,y)=\sum_{n=-\infty}^{n=+\infty}\varphi^{(n)}(y)\mathrm{e}^{\mathrm{i}n\alpha x},\quad \theta_1(x,y)=\sum_{n=-\infty}^{n=+\infty}\phi^{(n)}(y)\mathrm{e}^{\mathrm{i}n\alpha x}, \tag{2.12a,b}$$

$$u_1(x,y)=\sum_{n=-\infty}^{n=+\infty}u_1^{(n)}(y)\mathrm{e}^{\mathrm{i}n\alpha x},\quad v_1(x,y)=\sum_{n=-\infty}^{n=+\infty}v_1^{(n)}(y)\mathrm{e}^{\mathrm{i}n\alpha x}, \tag{2.12c,d}$$

$$p_1(x,y)=Ax+\sum_{n=-\infty}^{n=+\infty}p_1^{(n)}(y)\mathrm{e}^{\mathrm{i}n\alpha x}, \tag{2.12e}$$

where $u_1^{(n)}=\mathrm{D}\varphi^{(n)}$, $v_1^{(n)}=-\mathrm{i}n\alpha\varphi^{(n)}$, $\varphi^{(n)}=\varphi^{(-n)*}$, $u_1^{(n)}=u_1^{(-n)*}$, $v_1^{(n)}=v_1^{(-n)*}$, $\phi^{(n)}=\phi^{(-n)*}$, $p_1^{(n)}=p_1^{(-n)*}$, and the asterisk denotes the complex conjugate. The products are expressed using Fourier expansions of the form

$$\langle u_1u_1\rangle=\sum_{n=-\infty}^{n=+\infty}\langle u_1u_1\rangle^{(n)}(y)\mathrm{e}^{\mathrm{i}n\alpha x},\quad \langle u_1v_1\rangle=\sum_{n=-\infty}^{n=+\infty}\langle u_1v_1\rangle^{(n)}(y)\mathrm{e}^{\mathrm{i}n\alpha x}, \tag{2.12f,g}$$

$$\langle v_1v_1\rangle=\sum_{n=-\infty}^{n=+\infty}\langle v_1v_1\rangle^{(n)}(y)\mathrm{e}^{\mathrm{i}n\alpha x}, \tag{2.12h}$$

$$\langle u_1\theta_1\rangle=\sum_{n=-\infty}^{n=+\infty}\langle u_1\theta_1\rangle^{(n)}(y)\mathrm{e}^{\mathrm{i}n\alpha x},\quad \langle v_1\theta_1\rangle=\sum_{n=-\infty}^{n=+\infty}\langle v_1\theta_1\rangle^{(n)}(y)\mathrm{e}^{\mathrm{i}n\alpha x}, \tag{2.12i,j}$$

$$\langle u_1\theta_0\rangle=\sum_{n=-\infty}^{n=+\infty}\langle u_1\theta_0\rangle^{(n)}(y)\mathrm{e}^{\mathrm{i}n\alpha x}. \tag{2.12k}$$

Substitution of (2.12) into (2.9) and separation of Fourier components results in a system of ordinary differential equations for the modal functions for $-\infty<n<\infty$ of the form

$$\mathrm{D}_n^2\varphi^{(n)}-\mathrm{i}n\alpha Re(u_0\mathrm{D}_n-\mathrm{D}^2u_0)\varphi^{(n)}-\mathrm{i}n\alpha Ra_p\phi^{(n)}=\mathrm{i}n\alpha Ra_pPr^{-1}\theta_0^{(n)}+N_\psi^{(n)}, \tag{2.13a}$$

$$\mathrm{D}_n\phi^{(n)}-\mathrm{i}n\alpha PrRe\,u_0\phi^{(n)}=\mathrm{i}n\alpha Re\,u_0\theta_0^{(n)}+N_{\theta0}^{(n)}+Pr\,N_{\theta1}^{(n)}, \tag{2.13b}$$

where $\mathrm{D}=\mathrm{d}/\mathrm{d}y$, $\mathrm{D}^2=\mathrm{d}^2/\mathrm{d}y^2$, $\mathrm{D}_n=\mathrm{D}^2-n^2\alpha^2$, $N_{\theta0}^{(n)}=\mathrm{i}n\alpha\langle u_1\theta_0\rangle^{(n)}+\mathrm{D}\langle v_1\theta_0\rangle^{(n)}$, $N_{\theta1}^{(n)}=\mathrm{i}n\alpha\langle u_1\theta_1\rangle^{(n)}+\mathrm{D}\langle v_1\theta_1\rangle^{(n)}$ and $N_\psi^{(n)}=\mathrm{i}n\alpha\mathrm{D}\langle u_1u_1\rangle^{(n)}+\mathrm{D}^2\langle u_1v_1\rangle^{(n)}+n^2\alpha^2\langle u_1v_1\rangle^{(n)}-\mathrm{i}n\alpha\mathrm{D}\langle v_1v_1\rangle^{(n)}$. The required boundary conditions and constraints for the modal

functions have the form

$$\mathrm{D}\varphi^{(n)}(\pm 1) = 0, \quad \varphi^{(n)}(\pm 1) = 0, \quad \phi^{(n)}(\pm 1) = 0 \quad \text{for } -\infty < n < +\infty, \qquad (2.14a\text{–}c)$$

where the conditions for $\varphi^{(0)}$ represent the stream function normalization condition and the flow-rate constraint. System (2.13) and (2.14) needs to be solved numerically.

For the purpose of numerical solution, the expansions (2.12) have been truncated after N_M terms. The discretization method in the y direction uses the Chebyshev collocation technique based on N_T collocation points. The resulting nonlinear algebraic system is solved using an iterative technique combined with under-relaxation of the form $\Phi_{j+1} = \Phi_j + \mathrm{RF}(\Phi_{comp} - \Phi_j)$, where $\Phi = \{\varphi^{(n)}, \phi^{(n)}\}$ is the vector of unknowns, Φ_{comp} denotes the current solution, Φ_j denotes the previous solution, Φ_{j+1} stands for the accepted value of the next iteration and RF denotes the relaxation factor. The solution process represents the first-order fixed point method, i.e. the full iteration step involves solution of (2.13) with the nonlinear terms on the right-hand side taken from the most recent iteration (they are ignored in the first iteration), evaluation of the new approximation of the velocity and temperature fields, and evaluation of the new values of the nonlinear terms. This process is continued until a convergence criterion in the form $\max(|\Phi_{comp} - \Phi_j|) < \mathrm{TOL}$ is satisfied, where TOL denotes the specified error. The number of collocation points and the number of Fourier modes used in the solution were selected through numerical experiments so that the flow quantities of interest were determined with at least six-digit accuracy. Typically $N_T = 50$ provided sufficient accuracy. The required value of N_M strongly depends on α, Re and Ra and can be as large as $N_M = 30$.

The evaluation of the nonlinear terms requires evaluation of products of two Fourier series. It is more efficient to evaluate these products in physical space rather than in Fourier space. The required quantities were computed in physical space on a suitable grid based on the collocation points in the y direction and on a uniformly distributed set of points in the x direction, and the relevant products were evaluated. The fast Fourier transform (FFT) algorithm was used to express these products in terms of Fourier expansions (2.12). The aliasing error was controlled using a discrete FFT transform with N_p rather than N_M points, where $N_p \geqslant 3N_M/2$.

2.3. *Description of the primary convection when the lower wall is heated*

Figure 2 illustrates typical flow patterns. The pattern for purely natural convection ($Re = 0$) consists of a pair of counter-rotating rolls with fluid rising above the hot spots (figure 2*a*). The introduction of forced convection results in the formation of stream tube meandering between separation bubbles whose origin can be traced to the convection rolls, e.g. see the flow pattern in figure 2(*b*) for $Re = 5$. A further increase of Re results in the removal of the separation bubbles (figure 2*c*) and nearly complete elimination of the transverse motion.

The main quantities of interest are the net heat transfer between the walls and the horizontal heat transfer along the heated wall. The former is expressed in terms of the average Nusselt number Nu_{av} based on the conductive temperature scale, i.e.

$$Nu_{av} = \frac{Pr}{\lambda} \int_0^{\lambda} (-\mathrm{D}\theta_1|_{y=-1})\, \mathrm{d}x = -Pr\, \mathrm{D}\phi^{(0)}|_{y=-1}. \qquad (2.15a)$$

The latter is measured by evaluating the periodic part of the heat flow coming out of the wall per half wavelength and is expressed in terms of the horizontal Nusselt

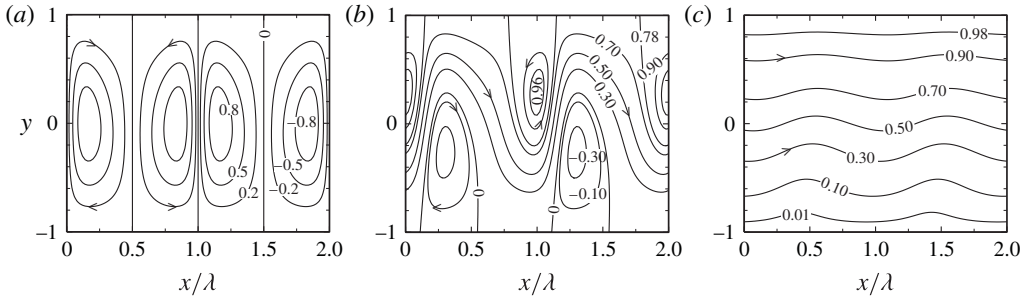

FIGURE 2. Flow patterns for $Ra_p = 1000$, $\alpha = 1$ and $Re = 0$ (a), 5 (b) and 20 (c), respectively. The complete stream function $\Psi(x, y) = Re(-y^3/3 + y + 2/3) + \psi(x, y)$ is normalized by its maximum, $\Psi_{max} = 6.52$ (a), 8.56 (b) and 26.27 (c), respectively.

number Nu_h defined as

$$\begin{aligned} Nu_h &= \frac{2}{\lambda} Pr \int_{-\lambda/4}^{\lambda/4} (-\mathrm{D}\theta_B|_{y=-1})\,\mathrm{d}x + Pr\mathrm{D}\phi^{(0)}|_{y=-1} \\ &= \frac{\alpha}{2\pi}[\coth(\alpha) + \tanh(\alpha)] + \left[\frac{2}{\lambda} Pr \int_{-\lambda/4}^{\lambda/4} (-\mathrm{D}\theta_1|_{y=-1})\,\mathrm{d}x + Pr\mathrm{D}\phi^{(0)}|_{y=-1}\right] \\ &= Nu_{h,cond} + Nu_{h,conv}. \end{aligned} \tag{2.15b}$$

In the above, the first term on the right-hand side accounts for the conductive heat flow, and the second accounts for the convective heat flow. The reader may note alternative methods for estimation of the horizontal heat fluxes (Maxworthy 1997; Siggers *et al.* 2004; Hughes & Griffiths 2008; Winters & Young 2009).

The qualitative analysis of Nu_{av} can be carried out by extracting mode zero from (2.13b), i.e.

$$\mathrm{D}^2\phi^{(0)} = \sum_{m=-\infty}^{m=\infty} \mathrm{D}[(\theta_0^{(-m)} + Pr\phi^{(-m)})v_1^{(m)}]. \tag{2.16a}$$

Double integration and application of the boundary conditions results in

$$\phi^{(0)} = M(y) - M(1)(1+y)/2, \quad M(y) = \int_{-1}^{y} \sum_{m=-\infty}^{m=\infty} (\theta_0^{(-m)}(\eta) + Pr\,\phi^{(-m)}(\eta))v_1^{(m)}(\eta)\,\mathrm{d}\eta \tag{2.16b,c}$$

and leads to

$$Nu_{av} = -Pr\,M(1)/2. \tag{2.17}$$

The function M can be referred to as the heat transport function and its form demonstrates explicitly the essential role played by the vertical velocity component in creating the net heat transfer. We shall now investigate how the convective motion is affected by the characteristics of the applied heating.

2.3.1. *Long-wavelength heating* ($\alpha \to 0$)

We begin the analysis by identifying the range of α that leads to the most intense heat transfer. In the case of long-wavelength heating ($\alpha \to 0$), the conductive field (i.e. (2.5)) can be approximated as

$$\theta_0(x, y) = [\theta_{00}(y) + \alpha^2\theta_{02}(y) + \alpha^4\theta_{04}(y) + O(\alpha^6)]\cos(X), \tag{2.18}$$

where the definitions of θ_{00}, θ_{02} and θ_{04} are given in appendix A and $X = \alpha x$ denotes the slow scale. The field equations, with x replaced by the slow scale, assume the form

$$\alpha(Re\,u_0 + u_1)\frac{\partial u_1}{\partial X} + Re\,v_1 \mathrm{D}u_0 + v_1\frac{\partial u_1}{\partial y} = -\alpha\frac{\partial p_1}{\partial X} + \alpha^2\frac{\partial^2 u_1}{\partial X^2} + \frac{\partial^2 u_1}{\partial y^2}, \tag{2.19a}$$

$$\alpha(Re\,u_0 + u_1)\frac{\partial v_1}{\partial X} + v_1\frac{\partial v_1}{\partial y} = -\frac{\partial p_1}{\partial y} + \alpha^2\frac{\partial^2 v_1}{\partial X^2} + \frac{\partial^2 v_1}{\partial y^2} + Ra_p\theta_1 + Ra_p Pr^{-1}\theta_0, \tag{2.19b}$$

$$(Re\,u_0 + u_1)\left(\alpha\frac{\partial \theta_0}{\partial X} + Pr\,\alpha\frac{\partial \theta_1}{\partial X}\right) + v_1\left(\frac{\partial \theta_0}{\partial y} + Pr\frac{\partial \theta_1}{\partial y}\right) = \alpha^2\frac{\partial^2 \theta_1}{\partial X^2} + \frac{\partial^2 \theta_1}{\partial y^2}, \tag{2.19c}$$

$$\alpha\frac{\partial u_1}{\partial X} + \frac{\partial v_1}{\partial y} = 0 \tag{2.19d}$$

and lead to a solution that can be represented as

$$[u_1(X, y),\, v_1(X, y),\, \theta_1(X, y)] = \sum_{n=1}^{4} \alpha^n [U_n(X, y),\, V_n(X, y),\, \Theta_n(X, y)] + O(\alpha^5), \tag{2.20a}$$

$$p_1(X, y) = \sum_{n=0}^{3} \alpha^n P_n(X, y) + O(\alpha^4), \quad [Nu_{av}, Nu_L] = \sum_{n=1}^{4} \alpha^n [Nu_{av,n}, Nu_{L,n}], \tag{2.20b,c}$$

where Nu_L is the local Nusselt number. The above expansions are substituted into (2.19), with the leading-order system being of the form

$$\frac{\partial^2 U_1}{\partial y^2} = \frac{\partial P_0}{\partial X}, \quad \frac{\partial P_0}{\partial y} = \frac{Ra_p}{Pr}\theta_{00}\cos(X), \quad \frac{\partial U_1}{\partial X} + \frac{\partial V_2}{\partial y} = 0, \quad \frac{\partial^2 \Theta_1}{\partial y^2} = -Re\,u_0\theta_{00}\sin(X), \tag{2.21a–d}$$

with the proper boundary conditions and the flow-rate constraint. The solution is of the form

$$U_1(X, y) = Ra_p Pr^{-1} F_{U1}(y)\sin(X), \quad V_2(X, y) = Ra_p Pr^{-1} F_{V2}(y)\cos(X), \tag{2.22a,b}$$

$$P_0(X, y) = Ra_p Pr^{-1} F_{P0}(y)\cos(X), \tag{2.22c}$$

$$\Theta_1(X, y) = ReF_{\Theta 1}(y)\sin(X), \quad Nu_{av,1} = 0, \quad Nu_{L,1} = -5^{-1} PrRe\sin(X), \tag{2.22d–f}$$

with definitions of F_{U1}, F_{V2}, F_{P0} and $F_{\Theta 1}$ given in appendix A. Here U_1, V_2 and P_0 describe the natural convection, which is unaffected by the forced convection at this level of approximation, and Θ_1 describes modifications of the temperature field created by the forced convection. There is no net heat transfer between the walls. The next-order system has the form

$$\frac{\partial^2 U_2}{\partial y^2} = \frac{\partial P_1}{\partial X} + Re\left(u_0\frac{\partial U_1}{\partial X} + \frac{\mathrm{d}u_0}{\mathrm{d}y}V_2\right), \quad \frac{\partial P_1}{\partial y} = Ra_p\Theta_1, \tag{2.23a,b}$$

$$\frac{\partial U_2}{\partial X} + \frac{\partial V_3}{\partial y} = 0, \quad \frac{\partial^2 \Theta_2}{\partial y^2} = RePr\,u_0\frac{\partial \Theta_1}{\partial X} - \theta_{00}U_1\sin(X) + \mathrm{D}\theta_{00}V_2\cos(X). \tag{2.23c,d}$$

A similar solution process leads to

$$U_2(X,y) = Ra_pRe[F_{U21}(y) + Pr^{-1}F_{U22}(y)]\cos(X), \tag{2.24a}$$

$$V_3(X,y) = Ra_pRe[F_{V31}(y) + Pr^{-1}F_{V32}(y)]\sin(X), \tag{2.24b}$$

$$P_1(X,y) = Ra_pRe[F_{P1}(y) - \tfrac{1}{1050}Pr^{-1}]\sin(X), \tag{2.24c}$$

$$\Theta_2(X,y) = Ra_pPr^{-1}F_{\Theta 21}(y) + Re^2Pr\,F_{\Theta 22}(y)\cos(X) + Ra_pPr^{-1}F_{\Theta 23}(y)\cos(2X), \tag{2.24d}$$

$$Nu_{av,2} = \tfrac{1}{1400}Ra_p, \quad Nu_{L,1} = \tfrac{1}{1400}Ra_p + [\tfrac{88}{1575}Pr^2\,Re^2 - \tfrac{3}{1400}Ra_p]\cos(X), \tag{2.24e,f}$$

with the definitions of F_{U21}, F_{U22}, F_{V31}, F_{V32}, F_{P1}, $F_{\Theta 21}$, $F_{\Theta 22}$ and $F_{\Theta 23}$ given in appendix A. Here F_{U21}, F_{V31} and F_{P1} arise because of temperature changes created by the forced convection, F_{U22}, F_{V32} and F_{P1} arise because of the interaction of the natural and forced convective motions, $F_{\Theta 22}$ accounts for the temperature changes created by the forced convection, and $F_{\Theta 21}$ and $F_{\Theta 23}$ account for changes in the conductive temperature field created by the natural convection. There is a net heat transfer between both walls at this level of approximation. The next-order system has the form

$$\frac{\partial^2 U_3}{\partial y^2} = \frac{\partial P_2}{\partial X} + Re\left(u_0\frac{\partial U_2}{\partial X} + \frac{\mathrm{d}u_0}{\mathrm{d}y}V_3\right) + U_1\frac{\partial U_1}{\partial X} + V_2\frac{\partial U_1}{\partial y} - \frac{\partial^2 U_1}{\partial X^2}, \tag{2.25a}$$

$$\frac{\partial P_2}{\partial y} = \frac{\partial^2 V_2}{\partial y^2} + Ra_p\Theta_2 + Ra_pPr^{-1}\theta_{02}\cos(X), \tag{2.25b}$$

$$\frac{\partial U_3}{\partial X} + \frac{\partial V_4}{\partial y} = 0, \tag{2.25c}$$

$$\frac{\partial^2 \Theta_3}{\partial y^2} = Re\left[Pr\,u_0\frac{\partial \Theta_2}{\partial X} - u_0\theta_{02}\sin(X)\right] + Pr\left(U_1\frac{\partial \Theta_1}{\partial X} + V_2\frac{\partial \Theta_1}{\partial y}\right) - U_2\theta_{00}\sin(X) + \mathrm{D}\theta_{00}V_3\cos(X) - \frac{\partial^2 \Theta_1}{\partial X^2}. \tag{2.25d}$$

Its solution can be written as

$$\begin{aligned} U_3 &= Ra_p\{Pr^{-1}F_{U31}(y) + Re^2[F_{U32}(y) + Pr^{-1}F_{U33}(y) + Pr\,F_{U34}(y)]\}\sin(X) \\ &\quad + Ra_p^2[Pr^{-1}F_{U35}(y) + Pr^{-2}F_{U36}(y)]\sin(2X), \end{aligned} \tag{2.26a}$$

$$\begin{aligned} V_4 &= Ra_p\{Pr^{-1}F_{V41}(y) + Re^2[F_{V42}(y) + Pr^{-1}F_{V43}(y) + Pr\,F_{V44}(y)]\}\cos(X) \\ &\quad + Ra_p^2[Pr^{-1}F_{V45}(y) + Pr^{-2}F_{V46}(y)]\cos(2X), \end{aligned} \tag{2.26b}$$

$$\begin{aligned} \Theta_3 &= \{Re\,F_{\Theta 31}(y) + Pr^2Re^3F_{\Theta 32}(y) + Ra_pRe[F_{\Theta 33}(y) + Pr^{-1}F_{\Theta 34}(y)]\}\sin(X) \\ &\quad + Ra_pRe[F_{\Theta 35}(y) + Pr^{-1}F_{\Theta 36}(y)]\sin(2X), \end{aligned} \tag{2.26c}$$

$$Nu_{av,3} = 0, \tag{2.26d}$$

$$\begin{aligned} Nu_{L,3} &= -[-\tfrac{17}{63}RePr + (\tfrac{47}{1039\,500} + \tfrac{169}{346\,500}Pr)Ra_pRe - \tfrac{5872}{307\,125}Pr^3Re^3]\sin(X) \\ &\quad + (\tfrac{47}{1039\,500} + \tfrac{111}{77\,000}Pr)Ra_pRe\,\sin(2X). \end{aligned} \tag{2.26e}$$

It is sufficient to consider only the energy equation at the next level of approximation in order to obtain a better approximation of the net heat transfer. This equation takes

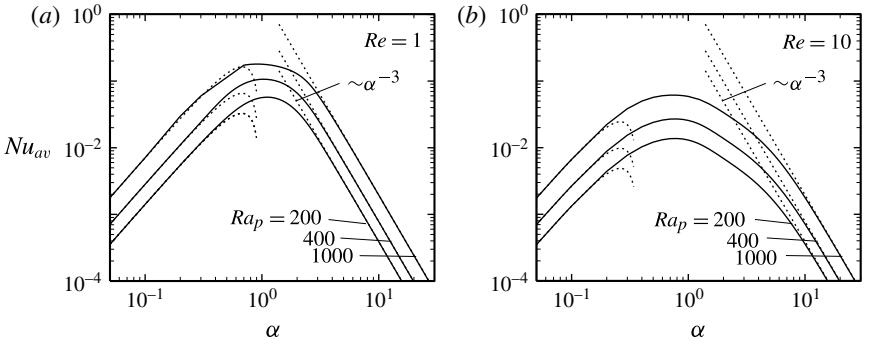

FIGURE 3. Variations of the average Nusselt number Nu_{av} as a function of α for $Ra_p = 200$, 400 and 1000 with $Re = 1$ (*a*) and $R = 10$ (*b*). The asymptotes for $\alpha \to 0$ and $\alpha \to \infty$ are marked using dotted lines. The curves for $Re = 0$ and $Re = 1$ overlap within the resolution of panel (*a*).

the form

$$\frac{\partial^2 \Theta_4}{\partial y^2} = RePr\, u_0 \frac{\partial \Theta_3}{\partial X} + Pr\left(U_1 \frac{\partial \Theta_2}{\partial X} + U_2 \frac{\partial \Theta_1}{\partial X} + V_2 \frac{\partial \Theta_2}{\partial y} + V_3 \frac{\partial \Theta_1}{\partial y}\right) - (\theta_{02} U_1 + \theta_{00} U_3)\sin(X) + (\mathrm{D}\theta_{02} V_2 + \mathrm{D}\theta_{00} V_4)\cos(X) - \frac{\partial^2 \Theta_2}{\partial X^2}. \quad (2.27)$$

The aperiodic term on the right-hand side is responsible for the net heat flow and it results in

$$Nu_{av,4} = -\tfrac{52}{70\,875} Ra_p - (\tfrac{821}{851\,350\,500} + \tfrac{313}{1277\,025\,750} Pr + \tfrac{184\,127}{2128\,376\,250} Pr^2) Ra_p Re^2. \quad (2.28)$$

The expression for $Nu_{L,4}$ is not given due to its length. The results displayed in figure 3 demonstrate that (2.20) provides a good approximation for Nu_{av} when $\alpha < 0.2$.

2.3.2. *Short-wavelength heating ($\alpha \to \infty$)*

In the case of the short-wavelength heating, the conductive temperature field, i.e. (2.5), can be approximated as

$$\theta_0 = [\tfrac{1}{2}\mathrm{e}^{-\alpha(1+y)} + O(\mathrm{e}^{-\alpha})]\cos(\alpha x). \quad (2.29)$$

The x variations of the buoyancy force are confined to a thin boundary layer adjacent to the lower wall, and the natural convection is confined to the same layer. All the field variables above the boundary layer can be functions of the vertical coordinate only. The solution is expressed as an expansion in terms of α^{-1} and using the method of matched asymptotic expansions leads to the determination of the expansion terms. It can be shown through matching with the inner solution that the outer solution can be simplified to the following form:

$$u_{1,outer}(x, y) = O(\alpha^{-4}), \quad v_{1,outer}(x, y) = 0, \quad (2.30a,b)$$

$$p_{1,outer}(x, y) = \alpha^{-3}\tilde{P}_3(y) + O(\alpha^{-4}), \quad \theta_{1,outer}(x, y) = \alpha^{-3}\tilde{\Theta}_3(y) + O(\alpha^{-4}). \quad (2.30c,d)$$

Similarly, the Nusselt number can be represented as

$$Nu_{av} = \alpha^{-3} Nu_{av,(-3)} + O(\alpha^{-4}). \quad (2.31)$$

Substitution of (2.29) and (2.30) into the field equations and separation of terms of equal order of magnitude leads to the following systems:

$$\frac{\partial \tilde{P}_3}{\partial y} = Ra_p \tilde{\Theta}_3, \quad \mathrm{D}^2\tilde{\Theta}_3 = 0, \tag{2.32a,b}$$

with solution of the form

$$\tilde{\Theta}_3 = \tilde{B}_3(y-1), \quad \tilde{P}_3 = Ra_p\tilde{B}_3\left(\frac{y^2}{2} - y\right), \tag{2.33a,b}$$

where $\tilde{B}_3$ is to be determined from matching with the inner solution. The heat transport in the outer zone is driven by the vertical conduction with a non-zero boundary condition at the edge of the boundary layer created by the boundary layer phenomena.

Analysis of the boundary layer begins with the introduction of the fast scale $\xi = \alpha x$ in the horizontal direction and the stretched coordinate centred at the lower wall $\eta = \alpha(1+y)$ in the vertical direction. The externally imposed temperature and velocity fields expressed in the (ξ, η) coordinate system have the form

$$\theta_0 = \frac{1}{2}\mathrm{e}^{-\eta}\cos(\xi), \quad \frac{\partial\theta_0}{\partial x} = -\alpha^{-1}\frac{1}{2}\mathrm{e}^{-\eta}\sin(\xi), \quad \frac{\partial\theta_0}{\partial y} = -\alpha^{-1}\frac{1}{2}\mathrm{e}^{-\eta}\cos(\xi), \tag{2.34a}$$

$$u_0 = \alpha^{-1}2\eta - \alpha^{-2}\eta^2, \quad \mathrm{D}u_0 = 2 - \alpha^{-1}2\eta. \tag{2.34b}$$

The field equations expressed in terms of the (ξ, η) system are of the form

$$\begin{aligned}\frac{\partial^2 u_1}{\partial\xi^2} + \frac{\partial^2 u_1}{\partial\eta^2} - \alpha^{-1}\frac{\partial p_1}{\partial\xi} &= \alpha^{-1}[Re(\alpha^{-1}2\eta - \alpha^{-2}\eta^2) + u_1]\frac{\partial u_1}{\partial\xi} \\ &\quad + \alpha^{-2}\left[Re(2 - \alpha^{-1}2\eta) + \alpha\frac{\partial u_1}{\partial\eta}\right]v_1, \qquad (2.35a)\\ \frac{\partial^2 v_1}{\partial\xi^2} + \frac{\partial^2 v_1}{\partial\eta^2} - \alpha^{-1}\frac{\partial p_1}{\partial\eta} &= \alpha^{-1}[Re\,(\alpha^{-1}2\eta - \alpha^{-2}\eta^2) + u_1]\frac{\partial v_1}{\partial\xi} + \alpha^{-1}v_1\frac{\partial v_1}{\partial\eta} \\ &\quad - \alpha^{-2}Ra_p\theta_1 + \alpha^{-2}\frac{1}{2}Ra_p Pr^{-1}\mathrm{e}^{-\eta}\cos(\xi), \qquad (2.35b)\\ \frac{\partial u_1}{\partial\xi} + \frac{\partial v_1}{\partial\eta} &= 0, \qquad (2.35c)\\ \frac{\partial^2\theta_1}{\partial\xi^2} + \frac{\partial^2\theta_1}{\partial\eta^2} &= \alpha^{-1}[Re\,(\alpha^{-1}2\eta - \alpha^{-2}\eta^2) + u_1]\left[-\frac{1}{2}\mathrm{e}^{-\eta}\sin(\xi) + Pr\frac{\partial\theta_1}{\partial\xi}\right] \\ &\quad + \alpha^{-2}v_1\left[-\frac{1}{2}\alpha\mathrm{e}^{-\eta}\cos(\xi) + \alpha\,Pr\frac{\partial\theta_1}{\partial\eta}\right]. \qquad (2.35d)\end{aligned}$$

The solution of (2.35) can be represented as

$$\begin{aligned}&[u_{1,inner}(\xi,\eta), v_{1,inner}(\xi,\eta), \theta_{1,inner}(\xi,\eta)] \\ &\quad = \sum_{n=2}^{3}\alpha^{-n}[U_n(\xi,\eta), V_n(\xi,\eta), \Theta_n(\xi,\eta)] + O(\alpha^{-4}), \qquad (2.36)\\ &p_{1,inner}(\xi,\eta) = \sum_{n=1}^{2}\alpha^{-n}P_n(\xi,\eta) + O(\alpha^{-3}). \qquad (2.37)\end{aligned}$$

Substitution of (2.36) and (2.37) into (2.35) and retention of the leading-order terms leads to a system of $O(\alpha^{-2})$ of the form

$$\frac{\partial^2 U_2}{\partial \xi^2}+\frac{\partial^2 U_2}{\partial \eta^2}-\frac{\partial P_1}{\partial \xi}=0, \quad \frac{\partial^2 V_2}{\partial \xi^2}+\frac{\partial^2 V_2}{\partial \eta^2}-\frac{\partial P_1}{\partial \eta}=\frac{1}{2}Ra_p Pr^{-1}\mathrm{e}^{-\eta}\cos(\xi), \quad (2.38a,b)$$

$$\frac{\partial U_2}{\partial \xi}+\frac{\partial V_2}{\partial \eta}=0, \quad \frac{\partial^2 \Theta_2}{\partial \xi^2}+\frac{\partial^2 \Theta_2}{\partial \eta^2}=-Re\eta\mathrm{e}^{-\eta}\sin(\xi). \quad (2.38c,d)$$

Its solution

$$U_2(\xi,\eta)=-\frac{Ra_p}{16Pr}(2\eta-\eta^2)\mathrm{e}^{-\eta}\sin(\xi), \quad V_2(\xi,\eta)=\frac{Ra_p}{16Pr}\eta^2\mathrm{e}^{-\eta}\cos(\xi), \quad (2.39a,b)$$

$$P_1(\xi,\eta)=-\frac{Ra_p}{8Pr}(3-2\eta)\mathrm{e}^{-\eta}\cos(\xi), \quad \Theta_2(\xi,\eta)=\frac{Re}{4}(\eta+\eta^2)\mathrm{e}^{-\eta}\sin(\xi) \quad (2.39c,d)$$

demonstrates that the natural convection is confined to the boundary layer and thus is unable to alter the net heat transfer between the walls. The system $O(\alpha^{-3})$ has the form

$$\frac{\partial^2 U_3}{\partial \xi^2}+\frac{\partial^2 U_3}{\partial \eta^2}-\frac{\partial P_2}{\partial \xi}=0, \quad \frac{\partial^2 V_3}{\partial \xi^2}+\frac{\partial^2 V_3}{\partial \eta^2}-\frac{\partial P_2}{\partial \eta}=0, \quad (2.40a,b)$$

$$\frac{\partial U_3}{\partial \xi}+\frac{\partial V_3}{\partial \eta}=0, \quad \frac{\partial^2 \Theta_3}{\partial \xi^2}+\frac{\partial^2 \Theta_3}{\partial \eta^2}=-\frac{1}{2}(-Re\eta^2+U_2)\mathrm{e}^{-\eta}\sin(\xi)-\frac{1}{2}V_2\mathrm{e}^{-\eta}\cos(\xi), \quad (2.40c,d)$$

and leads to the solution

$$U_3(\xi,\eta)=0, \quad V_3(\xi,\eta)=0, \quad P_2(\xi,\eta)=0, \quad (2.41a\text{–}c)$$

$$\Theta_3(\xi,\eta) = \left[\frac{Ra_p}{256Pr}+B_3\eta-\frac{Ra_p}{256Pr}(1+2\eta+2\eta^2)\mathrm{e}^{-2\eta}\right] - \frac{Re}{4}\left(\frac{\eta}{2}+\frac{\eta^2}{2}+\frac{\eta^3}{3}\right)\mathrm{e}^{-\eta}\sin(\xi)+\frac{Ra_p}{256Pr}\left(\frac{\eta}{2}+\eta^2\right)\mathrm{e}^{-2\eta}\cos(2\xi). \quad (2.41d)$$

Constant B_3 is determined from matching with the outer solution, leading to the uniformly valid expression for the temperature, i.e.

$$\theta_1(x,y) = \alpha^{-3}\left[\frac{Ra_p}{512Pr}(1-y)-\frac{Ra_p}{256Pr}[1+2\alpha(1+y)+2\alpha^2(1+y)^2]\mathrm{e}^{-2\alpha(1+y)} - \frac{Re}{4}\left[\frac{1}{2}\alpha(1+y)+\frac{1}{2}\alpha^2(1+y)^2+\frac{1}{3}\alpha^3(1+y)^3\right]\mathrm{e}^{-\alpha(1+y)}\sin(\alpha x) + \frac{Ra_p}{256\,Pr}\left[\frac{1}{2}\alpha(1+y)+\alpha^2(1+y)^2\right]\mathrm{e}^{-2\alpha(1+y)}\cos(2\alpha x)\right]+O(\alpha^{-4}). \quad (2.42)$$

The above expression demonstrates explicitly that the outer zone sees the edge of the boundary layer as a uniformly heated wall. The net heat transfer between the two walls can now be expressed as

$$Nu_{av}=\alpha^{-3}Ra_p/512+O(\alpha^{-4}). \quad (2.43)$$

The above expression provides a good approximation for Nu_{av} when $\alpha > 7$ (see figure 3).

2.3.3. *Weak heating*

The above discussion demonstrates, together with the results presented in figure 3, that the net heat transfer becomes marginal if the heating wavelength is either too short or too long. We shall now consider a heating wavelength $O(1)$. The heat transfer occurs due to the vertical fluid movement, as demonstrated in § 2.3. The forced motion increases the horizontal fluid movement, which competes with the vertical movement. A very strong horizontal motion may negate any transverse motion and thus may alter the heat transport qualitatively. It is convenient to start discussion of these processes by considering weak heating.

The natural convection is driven by nonlinear effects and thus its strength is not directly related to the magnitude of Ra_p; Ra_p of order $O(1)$ may generate convection with negligible nonlinear interactions. In the following analysis, the strength of the natural convection is measured using $\varepsilon \ll 1$. The flow quantities are represented as expansions in powers of ε of the form

$$(u_1, v_1, p_1, \theta_1) = \varepsilon(U_1, V_1, P_1, \Theta_1) + \varepsilon^2(U_2, V_2, P_2, \Theta_2) + O(\varepsilon^3). \tag{2.44}$$

Substitution of (2.44) into (2.6) and retention of the terms of the two highest orders of magnitude lead to a system $O(\varepsilon)$ of the form

$$\nabla^2 U_1 - Re\, u_0 \frac{\partial U_1}{\partial x} - Re\, V_1 \mathrm{D}u_0 - \frac{\partial P_1}{\partial x} = 0, \tag{2.45a}$$

$$\nabla^2 V_1 - Re\, u_0 \frac{\partial V_1}{\partial x} - \frac{\partial P_1}{\partial y} = -Ra_p\, \Theta_1 - Ra_p\, Pr^{-1} \hat{\theta}_0, \tag{2.45b}$$

$$\nabla^2 \Theta_1 - PrRe\, u_0 \frac{\partial \Theta_1}{\partial x} = Re\, u_0 \frac{\partial \hat{\theta}_0}{\partial x}, \tag{2.45c}$$

$$\frac{\partial U_1}{\partial x} + \frac{\partial V_1}{\partial y} = 0, \tag{2.45d}$$

where $\hat{\theta}_0 = \theta_0/\varepsilon = O(1)$, and a system $O(\varepsilon^2)$ of the form

$$\nabla^2 U_2 - Re\, u_0 \frac{\partial U_2}{\partial x} - Re\, V_2 \mathrm{D}u_0 - \frac{\partial P_2}{\partial x} = U_1 \frac{\partial U_1}{\partial x} + V_1 \frac{\partial U_1}{\partial y}, \tag{2.46a}$$

$$\nabla^2 V_2 - Re\, u_0 \frac{\partial V_2}{\partial x} - \frac{\partial P_2}{\partial y} = -Ra_p\, \Theta_2 + U_1 \frac{\partial V_1}{\partial x} + V_1 \frac{\partial V_1}{\partial y}, \tag{2.46b}$$

$$\nabla^2 \Theta_2 - PrRe\, u_0 \frac{\partial \Theta_2}{\partial x} = U_1 \frac{\partial \hat{\theta}_0}{\partial x} + V_1 \frac{\partial \hat{\theta}_0}{\partial y} + Pr\, U_1 \frac{\partial \Theta_1}{\partial x} + Pr\, V_1 \frac{\partial \Theta_1}{\partial y}, \tag{2.46c}$$

$$\frac{\partial U_2}{\partial x} + \frac{\partial V_2}{\partial y} = 0. \tag{2.46d}$$

Both systems are supplemented by the homogeneous boundary conditions and constraints resulting from (2.8).

The solution process starts with the energy equation (2.45*c*), which is decoupled from the rest of the system. Since ε is undefined, this equation is rearranged into the form

$$\nabla^2 \tilde{\Theta}_1 - PrRe\, u_0 \frac{\partial \tilde{\Theta}_1}{\partial x} = Re\, u_0 \frac{\partial \theta_0}{\partial x}, \tag{2.47}$$

where $\tilde{\Theta}_1 = \varepsilon\Theta_1$. The known forcing on the right-hand side of (2.47) leads to a solution of the form

$$\tilde{\Theta}_1(x, y) = \tilde{\Theta}_1^{(1)}(y)\mathrm{e}^{\mathrm{i}\alpha x} + \text{c.c.}, \tag{2.48}$$

where $\tilde{\Theta}_1^{(1)}$ is defined by the following problem,

$$\mathrm{D}^2\tilde{\Theta}_1^{(1)} - (\alpha^2 + \mathrm{i}\alpha Pr\, Re\, u_0)\tilde{\Theta}_1^{(1)} = \mathrm{i}\alpha Re\, u_0\theta_0^{(1)}, \quad \tilde{\Theta}_1^{(1)}(\pm 1) = 0, \tag{2.49a,b}$$

and c.c. stands for the complex conjugate. The solution has been determined using the spectral collocation method identical to that described in § 2.2. Determination of the net heat transfer requires analysis of the next-order problem, i.e. (2.46*c*). The coefficients of (2.46*c*) include the U_1 and V_1 velocity components, which need to be determined from the solution of (2.45*a*,*b*,*d*). Introduction of the stream function, defined as $u_1 = \partial\psi/\partial y$ and $v_1 = -\partial\psi/\partial x$, and elimination of the pressure results in a single equation of the form

$$\mathrm{D}^4\psi - Re\, u_0\left(\frac{\partial^3\psi}{\partial x\partial y^2} + \frac{\partial^3\psi}{\partial x^3}\right) + Re\,\mathrm{D}^2u_0\frac{\partial\psi}{\partial x} = Ra_p\frac{\partial\Theta_1}{\partial x} + Ra_p\, Pr^{-1}\frac{\partial\hat{\theta}_0}{\partial x}. \tag{2.50}$$

The character of the forcing on the right-hand side of (2.50) suggests a solution of the form

$$\varepsilon\psi(x, y) = \tilde{\psi}(x, y) = \tilde{\varphi}^{(1)}(y)\mathrm{e}^{\mathrm{i}\alpha x} + \text{c.c.} \tag{2.51}$$

Substitution of (2.5), (2.48) and (2.49) into (2.50) leads to the problem

$$\begin{aligned}\mathrm{D}^4\tilde{\varphi}^{(1)} - (2\alpha^2 + \mathrm{i}\alpha\, Re\, u_0)\mathrm{D}^2\tilde{\varphi}^{(1)} + (\alpha^4 + \mathrm{i}\alpha^3 Re\, u_0 + \mathrm{i}\alpha\, Re\,\mathrm{D}^2u_0)\tilde{\varphi}^{(1)} \\ = \mathrm{i}\alpha\, Ra_p\,\tilde{\Theta}_1^{(1)} + \mathrm{i}\alpha\, Ra_p Pr^{-1}\theta_0^{(1)}, \qquad (2.52a)\end{aligned}$$

$$\tilde{\varphi}^{(1)}(\pm 1) = \mathrm{D}\tilde{\varphi}^{(1)}(\pm 1) = 0, \tag{2.52b}$$

which describes the modal function $\tilde{\varphi}^{(1)}$. The solution of (2.52) can be determined using the spectral collocation method described in § 2.2. The corresponding velocity components can be expressed in the form

$$\varepsilon U_1 = \tilde{U}_1 = \varepsilon\frac{\partial\psi}{\partial y} = \frac{\partial\tilde{\psi}}{\partial y} = \mathrm{D}\tilde{\varphi}^{(1)}(y)\mathrm{e}^{\mathrm{i}\alpha x} + \text{c.c.} = \tilde{U}_1^{(1)}(y)\mathrm{e}^{\mathrm{i}\alpha x} + \text{c.c.}, \tag{2.53a}$$

$$\varepsilon V_1 = \tilde{V}_1 = \varepsilon\frac{\partial\psi}{\partial x} = \frac{\partial\tilde{\psi}}{\partial x} = \mathrm{i}\alpha\tilde{\varphi}^{(1)}(y)\mathrm{e}^{\mathrm{i}\alpha x} + \text{c.c.} = \tilde{V}_1^{(1)}(y)\mathrm{e}^{\mathrm{i}\alpha x} + \text{c.c.}, \tag{2.53b}$$

which is convenient for determination of the temperature correction $O(\varepsilon^2)$. Equation (2.46*c*) is arranged into the form

$$\nabla^2\tilde{\Theta}_2 - PrRe\, u_0\frac{\partial\tilde{\Theta}_2}{\partial x} = U_1\frac{\partial\hat{\theta}_0}{\partial x} + V_1\frac{\partial\hat{\theta}_0}{\partial y} + Pr\, U_1\frac{\partial\tilde{\Theta}_1}{\partial x} + Pr\, V_1\frac{\partial\tilde{\Theta}_1}{\partial y}, \tag{2.54}$$

where $\tilde{\Theta}_2 = \varepsilon\Theta_2$ and the right-hand side represents the known forcing $F(x, y)$, which can be written explicitly as

$$F(x, y) = F^{(0)}(y) + [F^{(2)}(y)\mathrm{e}^{2\mathrm{i}\alpha x} + \text{c.c.}], \tag{2.55a}$$

where

$$F^{(0)}(y) = [\mathrm{i}\alpha(\theta_0^{(1)} + Pr\,\tilde{\Theta}_1^{(1)})U_1^{(-1)} + (\mathrm{D}\theta_0^{(1)} + Pr\,\mathrm{D}\tilde{\Theta}_1^{(1)})V_1^{(-1)} + \mathrm{c.c.}], \quad (2.55b)$$

$$F^{(2)}(y) = [\mathrm{i}\alpha(\theta_0^{(1)} + Pr\,\tilde{\Theta}_1^{(1)})U_1^{(1)} + (\mathrm{D}\theta_0^{(1)} + Pr\,\mathrm{D}\tilde{\Theta}_1^{(1)})V_1^{(1)}]. \quad (2.55c)$$

The solution of (2.54) has the form

$$\tilde{\Theta}_2(x, y) = \tilde{\Theta}_2^{(0)}(y) + (\tilde{\Theta}_2^{(2)}(y)\mathrm{e}^{2\mathrm{i}\alpha x} + \mathrm{c.c.}), \quad (2.56)$$

i.e. it consists of a non-periodic term, which determines the net heat flow, and the first superharmonic of the imposed heating. Substitution of (2.55) and (2.56) into (2.54) and mode separation leads to equations for the modal functions of the form

$$\mathrm{D}^2\tilde{\Theta}_2^{(0)} = F^{(0)}, \quad \tilde{\Theta}_2^{(0)}(\pm 1) = 0, \quad (2.57a,b)$$

$$\mathrm{D}^2\tilde{\Theta}_2^{(2)} - 2\mathrm{i}\alpha\, RePr\, u_0\tilde{\Theta}_2^{(2)} = F^{(2)}, \quad \tilde{\Theta}_2^{(2)}(\pm 1) = 0. \quad (2.58a,b)$$

Before attempting solution, (2.57) is rearranged, i.e.

$$\mathrm{D}^2(\varepsilon\tilde{\Theta}_2^{(0)}) = \mathrm{D}(M^{(0)}), \quad (2.59a)$$

$$M^{(0)}(y) = [\theta_0^{(1)}\tilde{V}_1^{(-1)} + \theta_0^{(-1)}\tilde{V}_1^{(1)} + Pr(\tilde{\Theta}_1^{(1)}\tilde{V}_1^{(-1)} + \tilde{\Theta}_1^{(-1)}\tilde{V}_1^{(1)})]. \quad (2.59b)$$

Since the function $M^{(0)}$ is available, integration and application of boundary conditions leads to a solution of the form

$$\varepsilon\tilde{\Theta}_2^{(0)} = \int_{-1}^{y} M^{(0)}\,\mathrm{d}y - \frac{1}{2}(y+1)\int_{-1}^{1} M^{(0)}\,\mathrm{d}y. \quad (2.60)$$

Explicit evaluations of (2.60) have been carried out using the fourth-order-accurate extension of the trapezoid rule. Similarly, (2.58) is arranged into the form

$$\mathrm{D}^2(\varepsilon\tilde{\Theta}_2^{(2)}) - 2\mathrm{i}\alpha\, RePr\, u_0(\varepsilon\tilde{\Theta}_2^{(2)}) = M^{(2)}, \quad (2.61a)$$

$$M^{(2)}(y) = -(\theta_0^{(1)} + Pr\,\tilde{\Theta}_1^{(1)})\mathrm{D}\tilde{V}_1^{(1)} + \tilde{V}_1^{(1)}\mathrm{D}(\theta_0^{(1)} + Pr\,\tilde{\Theta}_1^{(1)}). \quad (2.61b)$$

The function $M^{(2)}$ is also available and thus solution of (2.61) can be determined; the spectral collocation method has been used for this purpose.

The average Nusselt number can be evaluated as

$$Nu_{av} = -Pr\,\frac{\mathrm{d}(\varepsilon\tilde{\Theta}_2^{(0)})}{\mathrm{d}y} = \frac{1}{2}\int_{-1}^{1} M^{(0)}\,\mathrm{d}y \quad (2.62)$$

without the need for an explicit determination of ε. The above analysis shows that Nu_{av} increases proportionally to Ra_p for small enough Ra_p. The approximation is sufficiently accurate for $Ra_p \approx 500$ as shown in figure 4.

Equation (2.62) demonstrates that the net heat flow results from the nonlinear effects associated with the buoyancy-driven motion. The heat transport function $M^{(0)}$ represents energy carried by the transverse movement of the fluid averaged over one heating wavelength in the x direction. Integration of this function between the walls gives the net energy transfer between the walls. The magnitude of $M^{(0)}$ depends on the magnitudes of $\theta_0^{(1)}$, $\tilde{\Theta}_1^{(1)}$ and $\tilde{V}_1^{(-1)}$ as well as on the phase difference between the temperature field and the vertical velocity component. The conductive temperature $\theta_0^{(1)}$ is always real, i.e. $\theta_0^{(1)} = \theta_0^{(-1)}$, while the phase of $\tilde{\Theta}_1^{(1)}$ changes depending on the strength of the forced motion.

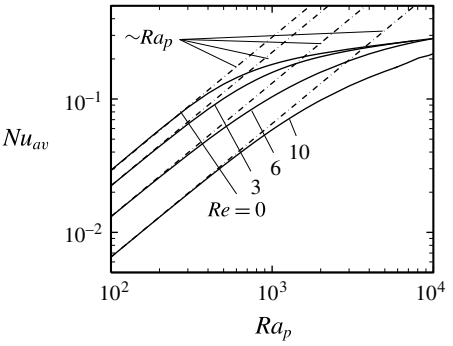

FIGURE 4. Variations of the average Nusselt number Nu_{av} as a function of Ra_p for $\alpha = 1$.

2.3.4. *Effects of the Reynolds number Re*

The introduction of a forced convection results in the formation of a continuous stream tube directed from left to right, which reduces the size of the rolls and separates vortex pairs into distinct objects that can be viewed as separation bubbles (see figure 2). The motion in the interior of these bubbles is driven by both the buoyancy and the shear created by the forced convection. The transverse motion, which is responsible for the vertical heat transfer, occurs in the interior of the bubbles as well as in the stream tube that meanders in the upwards and downwards directions. An increase of Re increases the size of the stream tube and makes this stream tube more rectilinear, and, as a result, the size of the rolls significantly decreases. The overall transverse motion decreases and the heat may be carried only by conduction across the stream tube.

The mechanics of the heat transfer changes as the presence of the forced motion modifies the temperature field (i.e. $\tilde{\Theta}_1^{(1)} \neq 0$ in (2.49)), alters the buoyancy-driven motion and changes the phase difference between the temperature and the vertical velocity component. We shall now discuss these processes in detail for the case of weak heating.

Assume initially that Re is small but finite. Separate $\tilde{\Theta}_1^{(1)}$ into real and imaginary parts and represent each as an expansion in terms of powers of Re, i.e.

$$\tilde{\Theta}_1^{(1)} = [Re\,\Theta_{r1} + Re^2\Theta_{r2} + O(Re^3)] + \mathrm{i}\,[Re\,\Theta_{i1} + Re^2\Theta_{i2} + O(Re^3)]. \tag{2.63}$$

Substitution of (2.63) into (2.49) and retention of terms proportional to the two lowest powers of Re results in the following systems:

$$O(Re): \qquad \mathrm{D}^2\Theta_{r1} - \alpha^2\Theta_{r1} = 0, \quad \mathrm{D}^2\Theta_{i1} - \alpha^2\Theta_{i1} = \alpha u_0\theta_0^{(1)}, \tag{2.64a,b}$$

$$O(Re^2): \qquad \mathrm{D}^2\Theta_{r2} - \alpha^2\Theta_{r2} = -\alpha\, Pr\, u_0\Theta_{i1}, \quad \mathrm{D}^2\Theta_{i2} - \alpha^2\Theta_{i2} = 0. \tag{2.65a,b}$$

Analysis of (2.64*a*) and (2.65*b*) shows that $\Theta_{r1} = 0$ and $\Theta_{i2} = 0$. The modification temperature $\tilde{\Theta}_1^{(1)}$ assumes non-zero values for small but finite Re, with its imaginary part playing the dominant role. Now separate the stream function into real and imaginary parts and represent them as expansions in terms of powers of Re, i.e.

$$\tilde{\varphi}^{(1)} = [\varphi_{r0} + Re\,\varphi_{r1} + Re^2\varphi_{r2} + O(Re^3)] + \mathrm{i}[\varphi_{i0} + Re\,\varphi_{i1} + Re^2\varphi_{i2} + O(Re^3)]. \tag{2.66}$$

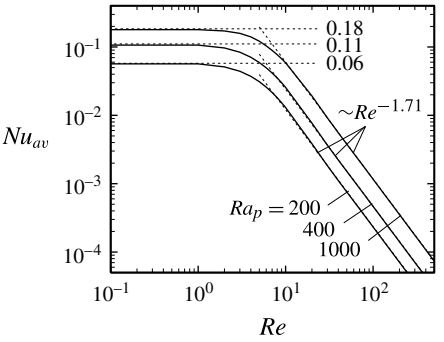

FIGURE 5. Variations of the average Nusselt number Nu_{av} as a function of Re for $\alpha = 1$ and $Ra_p = 200$, 400 and 1000. The asymptotes for $Re \to 0$ and $Re \to \infty$ are marked using dotted lines.

Substitution of (2.66) into (2.52) and retention of those terms proportional to the two lowest powers of Re results in the following systems:

$$O(Re^0): \qquad \mathrm{D}^4\varphi_{r0} - 2\alpha^2\mathrm{D}^2\varphi_{r0} + \alpha^4\varphi_{r0} = 0, \tag{2.67a}$$

$$\mathrm{D}^4\varphi_{i0} - 2\alpha^2\mathrm{D}^2\varphi_{i0} + \alpha^4\varphi_{i0} = \alpha\, Ra_p Pr^{-1}\theta_0^{(1)}, \tag{2.67b}$$

$$O(Re^1): \qquad \mathrm{D}^4\varphi_{r1} - 2\alpha^2\mathrm{D}^2\varphi_{r1} + \alpha^4\varphi_{r1} = -\alpha u_0 \mathrm{D}^2\varphi_{i0} + (\alpha^3 u_0 + \alpha \mathrm{D}^2 u_0)\varphi_{i0}, \tag{2.68a}$$

$$\mathrm{D}^4\varphi_{i1} - 2\alpha^2\mathrm{D}^2\varphi_{i1} + \alpha^4\varphi_{i1} = 0. \tag{2.68b}$$

Analysis of (2.67*a*) and (2.68*b*) shows that $\varphi_{r0} = 0$ and $\varphi_{i1} = 0$. Explicit evaluation of Θ_{i1}, Θ_{r2}, φ_{i0} and φ_{r1}, which requires numerical work, is not required for the further discussion. The temperature and the vertical velocity component have the forms

$$\theta_0^{(1)} + Pr\,\tilde{\Theta}_1^{(1)} = [\theta_0^{(1)} + Re^2 Pr\,\Theta_{r2} + O(Re^4)] + \mathrm{i}\,[RePr\Theta_{i1} + O(Re^3)], \tag{2.69a}$$

$$\tilde{V}_1^{(1)} = [\alpha\varphi_{i0} + \alpha\varphi_{i2}Re^2 + O(Re^4)] + \mathrm{i}\,[-\alpha\, Re\,\varphi_{r1} + O(Re^3)] \tag{2.69b}$$

and the heat transport function becomes

$$\begin{aligned} M^{(0)} &= 2\mathrm{Real}[(\theta_0^{(1)} + Pr\,\tilde{\Theta}_1^{(1)})\tilde{V}_1^{(-1)}] \\ &= 2\alpha\theta_0^{(1)}\varphi_{i0} + 2\,Re^2\alpha(\theta_0^{(1)}\varphi_{i2} + Pr\Theta_{r2}\varphi_{i0} - Pr\Theta_{i1}\varphi_{r1}) + O(Re^4). \end{aligned} \tag{2.70}$$

The forced motion affects both the temperature and the velocity fields at $O(Re)$ but these changes contribute only to a small phase shift and thus do not affect the heat flow. The heat flow is affected at $O(Re^2)$ and the change occurs due to (i) correction in the vertical velocity component that is in phase with the conductive field (the first term in the brackets in (2.70)), (ii) the part of the temperature modification that is in phase with the conductive temperature field (the second term in the brackets), and (iii) interaction between the parts of the velocity and temperature modifications that are out of phase with the conductive temperature field (the third term in the brackets). The importance of the third term is expected to rise as Re increases. The conclusion that the heat transfer approaches a constant limit corresponding to the pure natural convection when $Re \to 0$ is supported by the results presented in figure 5.

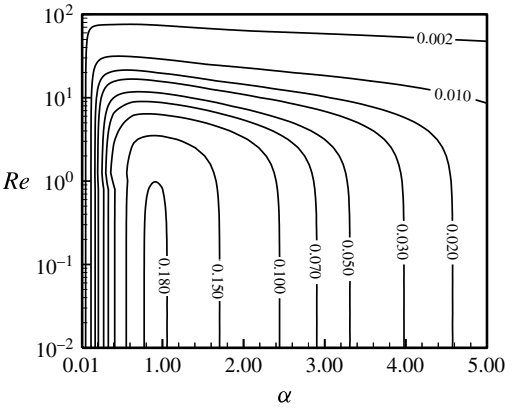

FIGURE 6. Variations of the average Nusselt number Nu_{av} as a function of α and Re for $Ra_p = 1000$.

Variations of the heat transport for large Re are more complex but can nevertheless be explained in qualitative terms. Equation (2.49) describing the temperature field has a variable coefficient containing the product Re and u_0, and an inhomogeneous term with a similar product. When $Re \to \infty$, these two terms are large everywhere except close to the walls where $u_0 \approx 0$ and thus temperature boundary layers may form. It can be shown that the temperature modal function $\tilde{\Theta}_1^{(1)} = (\Theta_r + \mathrm{i}\Theta_i)$ is equal to the conductive temperature modal function, i.e.

$$\tilde{\Theta}_1^{(1)} = (\Theta_r + \mathrm{i}\Theta_i) \approx -Pr^{-1}\theta_0^{(1)}, \tag{2.71}$$

everywhere except near the lower wall; this is due to the fact that $\theta_0^{(1)} \to 0.5$ but $\Theta_r \to 0$ when $y \to -1$. This leads to the formation of the temperature boundary layer at the lower wall. The flow becomes nearly isothermal outside the boundary layer, leading to the elimination of the buoyancy force in the bulk of the fluid. This force must overcome dissipation in the whole flow domain in order to drive natural convection. Clearly, the intensity of this convection must be decreasing rapidly as Re increases. As a result, the Nusselt number must also be decreasing. This process is illustrated in figure 5, where the numerically determined decrease rate is proportional to $Re^{-1.71}$ for $Re \to \infty$.

2.3.5. *Mixed convection under arbitrary heating conditions*

We shall now consider mixed convection for an arbitrary combination of transport parameters. The discussion presented in the previous sections demonstrate that Nu_{av} rapidly decreases for large Re and both small and large α. This defines the range of parameters that are relevant for potential applications. Figure 6 illustrates variations of Nu_{av} as a function of Re and α and clearly identifies the magnitudes of the net heat transfer driven by periodic heating. Figure 7 illustrates variations of Nu_{av} as a function of α and Ra_p for fixed Re and defines the conditions under which secondary motions are expected to set in. Figure 8 illustrates the magnitude of the horizontal heat flux and demonstrates that the overall heat flux is dominated by the conductive effects. The convective part of this flux ($Nu_{h,conv}$) has a similar magnitude and characteristics as Nu_{av}.

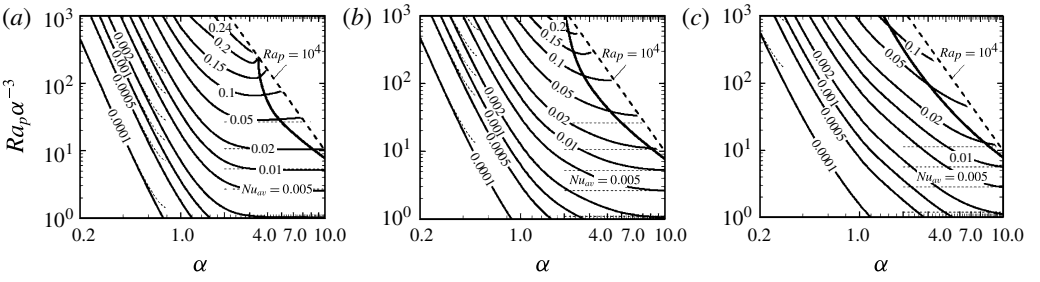

FIGURE 7. Variations of the average Nusselt number Nu_{av} as a function of $Ra_p\alpha^{-3}$ and α for $Re = 1$ (*a*), 5 (*b*) and 10 (*c*). The thick solid lines identify the critical stability conditions for the transverse rolls.

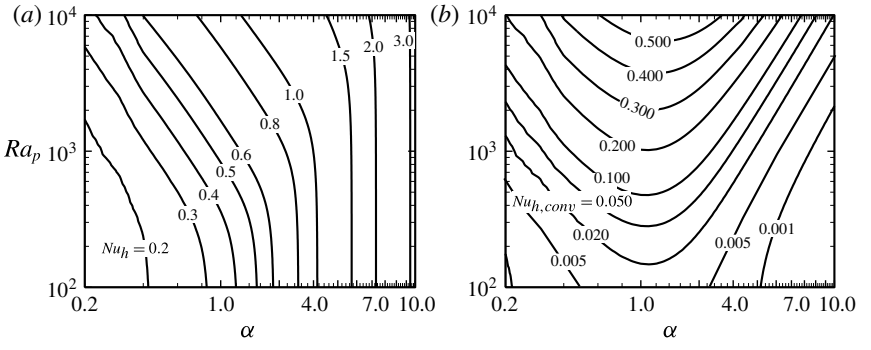

FIGURE 8. Variations of (*a*) the horizontal heat flux along the heated wall expressed in terms of the horizontal Nusselt number Nu_h and (*b*) the convective part of this heat flux expressed in terms of the horizontal convective Nusselt number $Nu_{h,conv}$.

2.4. *Heating applied at the upper wall*

Consider the same problem as discussed above but apply the external heating at the upper wall. The conduction problem (2.4) needs to be replaced by

$$\nabla^2\theta_0 = 0, \quad \theta_0(+1) = \tfrac{1}{2}\cos(\alpha x), \quad \theta_0(-1) = 0, \tag{2.72a–c}$$

while the rest of the formulation remains the same. The similarity of the flow response to that found in the case of heating applied from below can be demonstrated by (i) reversing the direction of gravity, i.e. $Ra_p \to -Ra_p$, and (ii) changing the sign of the temperature, i.e. $\theta \to -\theta$. The latter condition implies a change of the sign of the temperature imposed at the lower plate and results in a shift of the temperature field by half a cycle in the x direction. As a result, the global convection characteristics for the system heated from above are identical to those found in the case of the system heated from below (Hossain & Floryan 2014).

3. Stability of the primary convection

The linear stability theory is used to identify the onset conditions and to predict the form of the secondary motions. We begin with convection resulting from heating applied at the lower wall.

3.1. *Problem formulation*

The stability analysis begins with the momentum equations written in the vorticity transport form supplemented by the energy and the continuity equations, i.e.

$$\frac{\partial \boldsymbol{\omega}}{\partial t} - (\boldsymbol{\omega}\cdot\boldsymbol{\nabla})\boldsymbol{v} + (\boldsymbol{v}\cdot\boldsymbol{\nabla})\boldsymbol{\omega} = \nabla^2\boldsymbol{\omega} + \boldsymbol{\nabla}\times(Ra_p\,\theta\,\boldsymbol{j}), \quad \boldsymbol{\nabla}\cdot\boldsymbol{v} = 0, \quad \boldsymbol{\omega} = \boldsymbol{\nabla}\times\boldsymbol{v}, \tag{3.1a–c}$$

$$\frac{\partial \theta}{\partial t} + (\boldsymbol{v}\cdot\boldsymbol{\nabla})\theta = Pr^{-1}\nabla^2\theta, \tag{3.1d}$$

where $\boldsymbol{j}$ is the unit vector along the vertical direction, and $\boldsymbol{\omega}$ and $\boldsymbol{v}$ are the vorticity and velocity vectors, respectively. Unsteady three-dimensional disturbances are superposed on the base flow in the form (Floryan 1997)

$$\boldsymbol{v} = \boldsymbol{v}_B(x, y) + \boldsymbol{v}_2(x, y, z, t), \quad \boldsymbol{\omega} = \boldsymbol{\omega}_B(x, y) + \boldsymbol{\omega}_2(x, y, z, t), \quad \theta = \theta_B(x, y) + \theta_2(x, y, z, t), \tag{3.2a–c}$$

where subscripts 2 refer to the disturbance fields, $\boldsymbol{v}_2 = (u_2, v_2, w_2)$ is the disturbance velocity vector, $\boldsymbol{\omega}_2 = (\omega_{x2}, \omega_{y2}, \omega_{z2})$ is the disturbance vorticity vector and θ_2 stands for the temperature disturbance. The flow quantities (3.2) are substituted into (3.1), the components containing the primary convection are subtracted, and the equations are linearized. The resulting disturbance equations have the form

$$\frac{\partial \boldsymbol{\omega}_2}{\partial t} + (\boldsymbol{v}_B\cdot\boldsymbol{\nabla})\boldsymbol{\omega}_2 - (\boldsymbol{\omega}_2\cdot\boldsymbol{\nabla})\boldsymbol{v}_B + (\boldsymbol{v}_2\cdot\boldsymbol{\nabla})\boldsymbol{\omega}_B - (\boldsymbol{\omega}_B\cdot\boldsymbol{\nabla})\boldsymbol{v}_2 = \nabla^2\boldsymbol{\omega}_2 + \boldsymbol{\nabla}\times(Ra_p\,\theta_2\boldsymbol{j}), \tag{3.3a}$$

$$\boldsymbol{\nabla}\cdot\boldsymbol{v}_2 = 0, \quad \boldsymbol{\omega}_2 = \boldsymbol{\nabla}\times\boldsymbol{v}_2, \quad \frac{\partial \theta_2}{\partial t} + (\boldsymbol{v}_2\cdot\boldsymbol{\nabla})\theta_B + (\boldsymbol{v}_B\cdot\boldsymbol{\nabla})\theta_2 = Pr^{-1}\nabla^2\theta_2, \tag{3.3b–d}$$

and are subject to the homogeneous boundary conditions

$$\boldsymbol{v}_2 = 0, \quad \theta_2 = 0 \tag{3.3e,f}$$

at the walls. The disturbance equations (3.3) have coefficients that are functions of x and y, and thus the solution can be written in the form

$$\boldsymbol{v}_2(x, y, z, t) = \boldsymbol{V}_2(x, y)\mathrm{e}^{\mathrm{i}(\delta x+\beta z-\sigma t)} + \text{c.c.}, \quad \boldsymbol{\omega}_2(x, y, z, t) = \boldsymbol{\Omega}_2(x, y)\mathrm{e}^{\mathrm{i}(\delta x+\beta z-\sigma t)} + \text{c.c.}, \tag{3.4a,b}$$

$$\theta_2(x, y, z, t) = \Theta_2(x, y)\mathrm{e}^{\mathrm{i}(\delta x+\beta z-\sigma t)} + \text{c.c.} \tag{3.4c}$$

The disturbance wavevector has components (δ, β) in the (x, z) directions, $\boldsymbol{V}_2(x, y)$, $\boldsymbol{\Omega}_2(x, y)$ and $\Theta_2(x, y)$ are the x-periodic amplitude functions modulated by the heating, the exponent σ is assumed to be complex ($\sigma = \sigma_r + \mathrm{i}\sigma_i$) with imaginary and real parts describing the rate of growth and the frequency of disturbances, respectively, and c.c. stands for the complex conjugate. Positive σ_i identifies instability.

The set (δ, β, σ) represents the eigenvalues for the specified heating conditions (Re, Pr, Ra_p, α), creating a large parameter space; the size of this space is reduced in this analysis by setting $Pr = 0.71$. The relevant eigenvalue problem for the partial differential equations (3.3) can be easily derived. Rather than solving this problem directly, we take advantage of the periodicity of the amplitude functions and represent them in terms of Fourier expansions

$$\boldsymbol{V}_2(x, y) = \sum_{m=-\infty}^{m=+\infty} [g_{2u}^{(m)}(y), g_{2v}^{(m)}(y), g_{2w}^{(m)}(y)]\mathrm{e}^{\mathrm{i}m\alpha x}, \tag{3.5a}$$

$$\boldsymbol{\Omega}_2(x,y)=\sum_{m=-\infty}^{m=+\infty}[\zeta_{2x}^{(m)}(y),\,\mathrm{i}\zeta_{2y}^{(m)}(y),\,\zeta_{2z}^{(m)}(y)]\mathrm{e}^{\mathrm{i}m\alpha x}, \tag{3.5b}$$

$$\Theta_2(x,y)=\sum_{m=-\infty}^{m=+\infty}g_{2\theta}^{(m)}(y)\mathrm{e}^{\mathrm{i}m\alpha x}, \tag{3.5c}$$

which leads to the following form of the disturbance quantities:

$$\boldsymbol{v}_2(x,y,z,t)\;=\;\sum_{m=-\infty}^{m=+\infty}[g_{2u}^{(m)}(y),\,g_{2v}^{(m)}(y),\,g_{2w}^{(m)}(y)]\mathrm{e}^{\mathrm{i}[(\delta+m\alpha)x+\beta z-\sigma t]}+\mathrm{c.c.}, \tag{3.6a}$$

$$\boldsymbol{\omega}_2(x,y,z,t)\;=\;\sum_{m=-\infty}^{m=+\infty}[\zeta_{2x}^{(m)}(y),\,\mathrm{i}\zeta_{2y}^{(m)}(y),\,\zeta_{2z}^{(m)}(y)]\mathrm{e}^{\mathrm{i}[(\delta+m\alpha)x+\beta z-\sigma t]}+\mathrm{c.c.}, \tag{3.6b}$$

$$\theta_2(x,y,z,t)\;=\;\sum_{m=-\infty}^{m=+\infty}g_{2\theta}^{(m)}(y)\mathrm{e}^{\mathrm{i}[(\delta+m\alpha)x+\beta z-\sigma t]}+\mathrm{c.c.} \tag{3.6c}$$

Substitution of (3.6) into (3.3) and separation of Fourier components results, after some rather lengthy algebra, in a system of linear homogeneous ordinary differential equations of the form

$$A^{(m)}\zeta_{2y}^{(m)}+Re\,\mathrm{D}u_0\beta g_{2v}^{(m)}=\sum_{n=-\infty}^{n=+\infty}[H_\zeta^{(m-n)}\zeta_{2y}^{(m-n)}+H_v^{(m-n)}g_{2v}^{(m-n)}], \tag{3.7a}$$

$$B^{(m)}g_{2v}^{(m)}-Ra_pk_m^2g_{2\theta}^{(m)}=-\sum_{n=-\infty}^{n=+\infty}[I_\zeta^{(m-n)}\zeta_{2y}^{(m-n)}+I_v^{(m-n)}g_{2v}^{(m-n)}], \tag{3.7b}$$

$$C^{(m)}g_{2\theta}^{(m)}=Pr\sum_{n=-\infty}^{n=+\infty}[J_\zeta^{(m-n)}\zeta_{2y}^{(m-n)}+J_v^{(m-n)}g_{2v}^{(m-n)}+J_\theta^{(m-n)}g_{2\theta}^{(m-n)}], \tag{3.7c}$$

subject to the boundary conditions

$$\zeta_{2y}^{(m)}(\pm1)=0,\quad g_{2v}^{(m)}(\pm1)=0,\quad \mathrm{D}g_{2v}^{(m)}(\pm1)=0,\quad g_{2\theta}^{(m)}(\pm1)=0\quad\text{for}\quad -\infty<m<+\infty, \tag{3.8a–d}$$

where

$$A^{(m)}=\mathrm{D}^2-k_m^2-\mathrm{i}(t_mRe\,u_0-\sigma), \tag{3.9a}$$

$$B^{(m)}=(\mathrm{D}^2-k_m^2)^2-\mathrm{i}(t_mRe\,u_0-\sigma)(\mathrm{D}^2-k_m^2)+\mathrm{i}t_mRe\,\mathrm{D}^2u_0, \tag{3.9b}$$

$$C^{(m)}=\mathrm{D}^2-k_m^2-\mathrm{i}\,Pr(t_mRe\,u_0-\sigma), \tag{3.10}$$

$$\mathrm{D}^n=\mathrm{d}^n/\mathrm{d}y^n, \tag{3.11}$$

$$t_m=\delta+m\alpha, \tag{3.12}$$

$$k_m^2=t_m^2+\beta^2, \tag{3.13}$$

$$H_\zeta^{(m-n)}=\mathrm{i}t_mu_1^{(n)}+k_{m-n}^{-2}(\beta^2+t_{m-n}t_m)v_1^{(n)}\mathrm{D}, \tag{3.14}$$

$$H_v^{(m-n)}=-\beta\mathrm{D}u_1^{(n)}+\mathrm{i}n\alpha\beta k_{m-n}^{-2}v_1^{(n)}\mathrm{D}^2, \tag{3.15}$$

$$I_\zeta^{(m-n)}=n\alpha\beta k_{m-n}^{-2}[2t_{m-n}u_1^{(n)}\mathrm{D}+(t_m+t_{m-n})\mathrm{D}u_1^{(n)}-\mathrm{i}k_m^2v_1^{(n)}-\mathrm{i}v_1^{(n)}\mathrm{D}^2], \tag{3.16}$$

$$I_v^{(m-n)} = k_{m-n}^{-2}[\mathrm{i}n\alpha(\beta^2 - t_m t_{m-n})\mathrm{D}u_1^{(n)}\mathrm{D} + k_m^2(\beta^2 + t_{m-n}t_{m-2n})v_1^{(n)}\mathrm{D}] + k_{m-n}^{-2}[\mathrm{i}(-k_{m-n}^2 t_m + 2n\alpha\beta^2)u_1^{(n)}\mathrm{D}^2 + (n\alpha t_m - k_m^2)v_1^{(n)}\mathrm{D}^3] + \mathrm{i}k_m^2 t_{m-2n}u_1^{(n)} + \mathrm{i}t_m\mathrm{D}^2 u_1^{(n)}, \tag{3.17}$$

$$J_\zeta^{(m-n)} = -\mathrm{i}n\alpha\beta k_{m-n}^{-2}\theta_B^{(n)}, \tag{3.18}$$

$$J_v^{(m-n)} = -n\alpha k_{m-n}^{-2}t_{m-n}\theta_B^{(n)}\mathrm{D} + \mathrm{D}\theta_B^{(n)}, \quad \theta_B^{(n)} = \phi^{(n)} + Pr^{-1}\delta_{1|n|}\theta_0^{(n)}, \tag{3.19a,b}$$

$$J_\theta^{(m-n)} = \mathrm{i}t_{m-n}u_1^{(n)} + v_1^{(n)}\mathrm{D}. \tag{3.20}$$

The above formulation is analogous to the Bloch theory (Bloch 1928) for systems with spatially periodic coefficients. It can also be interpreted in terms of the Floquet theory (Coddington & Levinson 1965).

3.2. *Method of solution*

Equations (3.7*a–c*), together with the boundary conditions (3.8), are truncated after N_M modes. The dispersion relation is determined numerically through solution of the relevant eigenvalue problem. For the purposes of calculations, the problem is posed as an eigenvalue problem for σ. Equations (3.7*a–c*) are discretized with spectral accuracy using the Chebyshev collocation method with N_T collocation points. The discretization procedure results in a matrix eigenvalue problem $\boldsymbol{\Xi}x = 0$, where $\boldsymbol{\Xi}(\sigma)$ represents the coefficient matrix. This matrix is linear in σ, i.e. $\boldsymbol{\Xi} = \boldsymbol{\Xi}_0 + \boldsymbol{\Xi}_1\sigma$, where $\boldsymbol{\Xi}_0 = \boldsymbol{\Xi}(0)$ and $\boldsymbol{\Xi}_1 = \boldsymbol{\Xi}(1) - \boldsymbol{\Xi}_0$. The σ spectrum is determined by solving a general eigenvalue problem of the form $\boldsymbol{\Xi}_0 x = \sigma\boldsymbol{\Xi}_1 x$. The individual eigenvalues are determined by finding the zeros of the determinant of $\boldsymbol{\Xi}$. The computed eigenvalues are further refined using the inverse iteration technique.

Two methods of tracing the eigenvalues in the parameter space have been used (Floryan 2003). In both of them we start with a small change of one of the dimensionless numbers. Then, in the first method, we produce an approximation for the eigenvalue, which is improved iteratively by searching for the nearby zero of the determinant using a Newton–Raphson search procedure. A reasonable guess for the unknown eigenvalue is essential for the convergence. In the second method, the inverse iterations method, we compute an approximation for the eigenvector $\boldsymbol{\Lambda}_a$ corresponding to the unknown eigenvalue σ_a using an iterative process in the form $(\boldsymbol{\Xi}_0 - \sigma_0\boldsymbol{\Xi}_1)\boldsymbol{\Lambda}^{(k+1)} = \boldsymbol{\Xi}_1\boldsymbol{\Lambda}^{(k)}$, where σ_0 and $\boldsymbol{\Lambda}^{(0)}$ are the eigenvalue and the eigenvector (an eigenpair) corresponding to the unaltered flow. If σ_a is the eigenvalue closest to σ_0, $\boldsymbol{\Lambda}^{(k)}$ converges to $\boldsymbol{\Lambda}_a$. The eigenvalue σ_a is evaluated using the formula $\sigma_a = \boldsymbol{\Lambda}_a^*\boldsymbol{\Xi}_0\boldsymbol{\Lambda}_a/\boldsymbol{\Lambda}_a^*\boldsymbol{\Xi}_1\boldsymbol{\Lambda}_a$, where the asterisk denotes the complex conjugate transpose. The inverse iterations method was found to be generally more efficient. The relevant numerical parameters (i.e. N_M and N_T) have been selected through numerical convergence studies to guarantee at least four-digit eigenvalue accuracy.

3.3. *Description of flow stability characteristics*

It is convenient to start the discussion with descriptions of two reference states, i.e. the natural convection ($Re = 0$) driven by periodic heating and the forced convection in a channel with a uniformly heated lower plate.

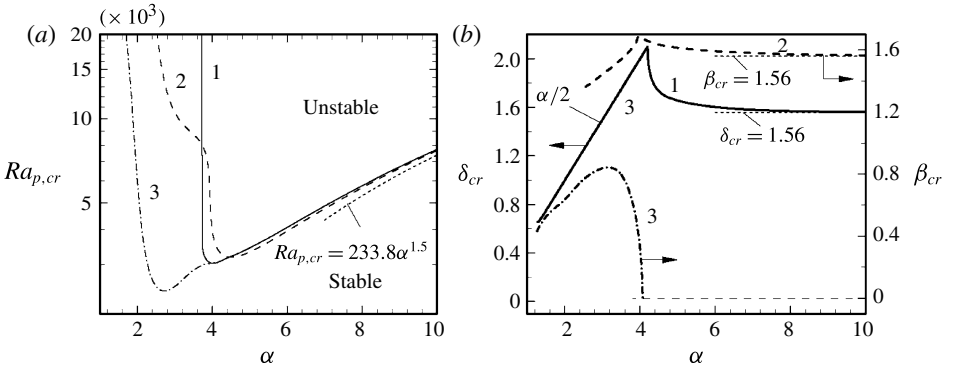

FIGURE 9. Variations of (*a*) the critical Rayleigh number $Ra_{p,cr}$ and (*b*) the critical wavenumbers δ_{cr} and β_{cr} as functions of α for the periodically heated layer with $Re = 0$ (see § 3.3.1). Curves 1, 2 and 3 correspond to the longitudinal, transverse and oblique rolls, respectively.

3.3.1. *Natural convection driven by a periodic heating* ($Re = 0$)

Two instability mechanisms are active in the case of periodic heating described by (2.1), i.e. the RB mechanism and the spatial parametric resonance mechanism (Hossain & Floryan 2013*b*). Three types of structures can be created at the onset, i.e. longitudinal rolls (rolls parallel to the primary rolls) driven primarily by the RB mechanism, transverse rolls (rolls orthogonal to the primary rolls) also driven primarily by the RB mechanism, and oblique rolls driven primarily by the spatial parametric resonance. Figure 9 illustrates variations of the critical Rayleigh number $Ra_{p,cr}$ and the critical wavenumbers δ_{cr} and β_{cr} as functions of α for these rolls. The oblique rolls play the critical role for $\alpha = O(1)$, the longitudinal rolls play such a role in a small interval of α centred around $\alpha \approx 4$ and the transverse rolls become critical for larger α. In the limit of $\alpha \to \infty$, the primary convection is confined to a thin boundary layer adjacent to the lower wall with the conduction state emerging above this layer (see § 2.3.2) resulting in the dominance of the RB mechanism. As a result, the critical stability curves approach an asymptote for $\alpha \to \infty$, which can be predicted on the basis of the RB instability (Pellew & Southwell 1940; Koschmieder 1993). Wavenumber lock-in between the primary rolls and the component of the disturbance wavevector parallel to the primary convection wavevector occurs for $\alpha = O(1)$.

3.3.2. *Forced convection driven by uniform heating*

Conditions leading to the onset of natural convection in the case of a uniformly heated lower wall and in the absence of forced convection are expressed in terms of the Rayleigh number defined as $Ra = g\Gamma h^3 \Delta T/\nu\kappa$, where ΔT stands for the temperature difference between the walls. The Rayleigh number Ra has to reach the critical value of $Ra_{cr} = 213.5$ in order to initiate any movement of the fluid (Pellew & Southwell 1940; Koschmieder 1993). The pattern of the resulting motion cannot be determined on the basis of linear stability theory; various symmetry-breaking mechanisms may affect this process (Freund, Pesch & Zimmermann 2011; Weiss, Seiden & Bodenschatz 2012). Introduction of forced motion provides another symmetry-breaking mechanism and gives preference to rolls with their axes parallel to the direction of the forced flow (Gage & Reid 1968). The evolution of the critical conditions as a function of Re is illustrated in figure 10. Three types of roll are

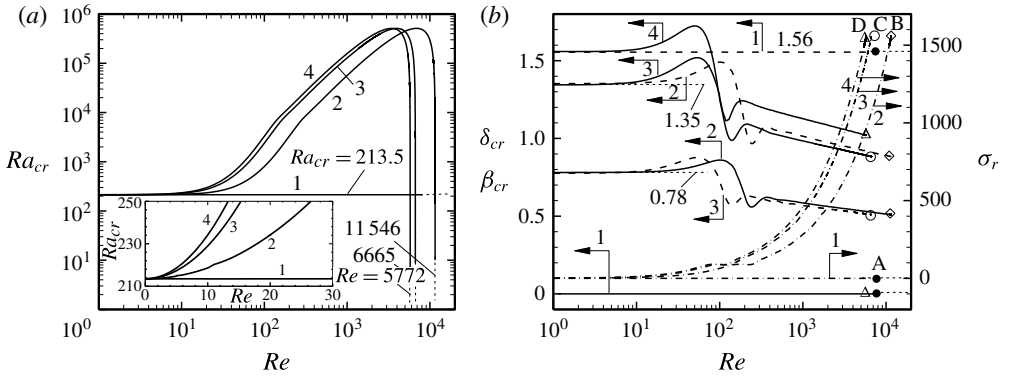

FIGURE 10. Variations of (*a*) the critical Rayleigh number Ra_{cr} and (*b*) the critical wavenumbers δ_{cr} and β_{cr}, and the frequency σ_r as functions of the Reynolds number Re for the uniformly heated fluid layer (see § 3.3.2). Curves 1, 2, 3 and 4 correspond to the parallel rolls, the 60° oblique rolls, the 30° oblique rolls, and the orthogonal rolls, respectively. In panel (*b*), the thick solid, dashed and dash-dotted lines identify δ_{cr}, β_{cr} and σ_r, respectively; the limit points A, B, C and D (marked using ●, ◇, ○, △) correspond to $(\delta_{cr}, \beta_{cr}, \sigma_r) = (0, 1.56, 0)$, $(0.51, 0.89, 1565)$, $(0.89, 0.51, 1554)$ and $(1.02, 0, 1554)$, respectively.

shown: (i) rolls with axes parallel to the flow direction are referred to as parallel rolls (they correspond to the transverse rolls in the case of periodic heating), (ii) rolls with axes orthogonal to the flow direction are referred to as orthogonal rolls (they correspond to the longitudinal rolls in the case of periodic heating), and (iii) oblique rolls. The obliqueness angle χ is defined as $\tan(\chi) = \beta/\delta$ and thus $\chi = 0°$ corresponds to orthogonal rolls and $\chi = 90°$ to parallel rolls. The critical conditions for all rolls approach the same limit of $Re_{cr} = 213.5$, $\sqrt{\delta_{cr}^2 + \beta_{cr}^2} = 1.56$, $\sigma_r = 0$ when $Re \to 0$. The critical conditions for the parallel rolls remain independent of Re and such rolls always remain stationary. All other rolls travel in the downstream direction when $Re > 0$ with σ_r increasing with Re; their Ra_{cr} increases with increase of Re, reaches a maximum and then drops off rapidly, as shown in figure 10. The orthogonal rolls are of the most interest as their Ra_{cr} drop to zero at the smallest Re, i.e. at $Re = 5772$, and this point corresponds to the shear instability beginning to play the critical role. The results displayed in figure 10 well illustrate the morphing of the orthogonal rolls into the two-dimensional Tollmien–Schlichting (TS) waves as Re increases. In summary, the parallel rolls play the critical role when $Re < 5772$, and the transition to the secondary state for such conditions is driven by the RB mechanism. The two-dimensional travelling waves play the critical role for $Re > 5772$, and for such conditions the transition is driven by viscous shear. One should note that flow with parallel rolls is subject to secondary instabilities (Clever & Busse 1991).

3.3.3. *Transverse rolls*

We shall now return to the periodic heating and enquire how the introduction of forced convection affects the onset conditions when compared with natural convection, and identify the form of the unstable motion at the onset. We begin the presentation with the transverse rolls; such rolls are parallel to the direction of the forced convection and are orthogonal to the primary rolls, and thus may exhibit some of the features of the parallel rolls generated by uniform heating. The form

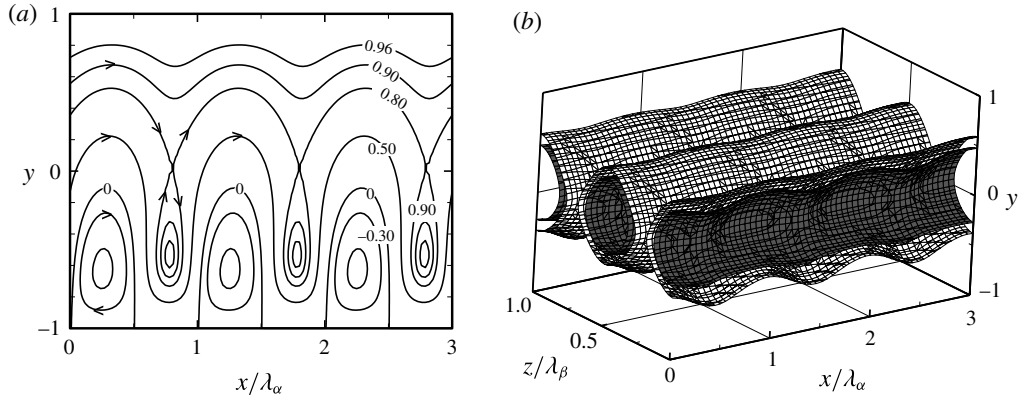

FIGURE 11. The flow structures associated with (*a*) the primary convection and (*b*) the secondary convection in the form of transverse rolls at the onset in a flow with $Re = 1$. (*a*) The stream function normalized by its maximum; (*b*) the second invariant of the velocity gradient tensor (see (3.21)). The heating has the wavenumber $\alpha = 5$, requires the intensity corresponding to $Ra_{p,cr} = 3317$ and generates the secondary convection with wavenumber $\beta_{cr} = 1.6$.

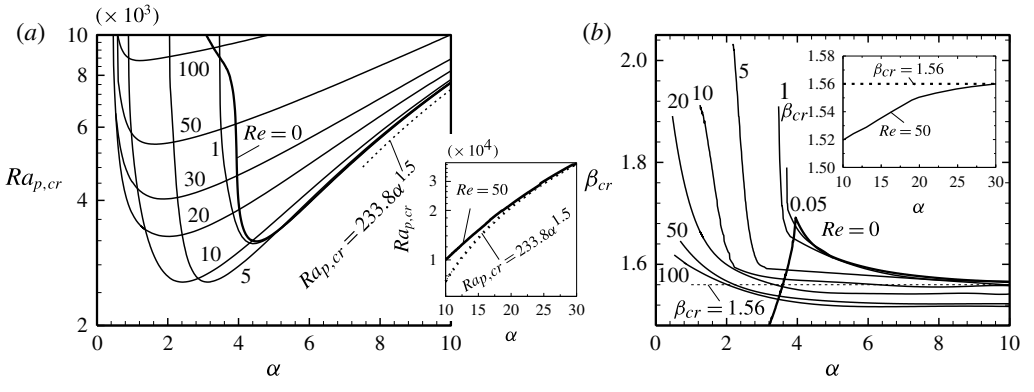

FIGURE 12. The onset conditions required for the formation of the secondary convection in the form of transverse rolls in the fluid flowing through a periodically heated channel at different Reynolds numbers *Re* (see § 3.3.3): variations of (*a*) the critical Rayleigh number Ra_{cr} and (*b*) the critical wavenumber β_{cr} as functions of the heating wavenumber α.

of these rolls is illustrated in figure 11, where the second invariant of the velocity gradient tensor ϑ (Dubief & Delcayre 2000), defined as

$$\vartheta = \tfrac{1}{2}(\Phi_{ij}\Phi_{ij} - \varpi_{ij}\varpi_{ij}), \tag{3.21}$$

where $\Phi_{ij} = (u_{i,j} - u_{j,i})/2$, $\varpi_{ij} = (u_{i,j} + u_{j,i})/2$, has been plotted with the disturbance velocity field normalized by the condition $\max(g^{(1)}_{2u}) = 1$. Figure 12(*a*) illustrates variations of Ra_{cr} as a function of α; the form of the critical curves suggests the existence of two characteristic zones. In the limit of $\alpha \to \infty$ these curves reach the same asymptote for all *Re* considered and, in this sense, the properties of these rolls resemble the properties of the parallel rolls of § 3.3.2. The asymptote can be

determined analytically by taking advantage of (2.43) (for details see Hossain & Floryan 2013*b*). This is due to the fact that in this limit the temperature field splits into a thin boundary layer adjacent to the heated wall and a conduction zone with a constant vertical temperature gradient above the boundary layer. As a result, the spatial parametric resonance is practically eliminated and the instability is driven by the RB mechanism. The results displayed in figure 12(*b*) demonstrate that the critical wavenumbers reach the limit $\beta_{cr} \to 1.56$ when $\alpha \to \infty$, which is identical to that found in the case of uniform heating. The situation is more complex when $\alpha = O(1)$, as the strength of the primary rolls is largest under such conditions (see § 2.3) and this strengthens the spatial parametric resonance. The critical curves displayed in figure 12(*a*) show large variations of form as a function of Re for $\alpha = O(1)$. A small increase of Re may destabilize the system and expand the unstable zone to smaller α values, but its further increase stabilizes the system due to the washing out of the separation bubbles, as illustrated in figures 2, 5 and 6. The complexity of this process is illustrated in figure 12(*b*), which displays variations of β_{cr} as a function of α for several values of Re. The strong role of the parametric resonance is underlined by the rapid change in the character of variations of β_{cr} for $Re = 0$ at $\alpha \approx 4$. Introduction of forced convection, regardless of how small Re might be, leads to the qualitative change in the variations of β_{cr} (figure 12*b*) and to an increase rather than a decrease of β_{cr} as the magnitude of α decreases to $\alpha < 4$.

Figure 13 illustrates effects of Re more explicitly. When $Re = O(1)$ and $\alpha = O(1)$, the parametric resonance is active and results in the formation of a variety of critical curves as shown in figure 13(*a*). An increase of Re while keeping Ra_p fixed results in the washing away of the primary rolls and the formation of a boundary layer at the lower wall (§ 2.3.4). These rolls can be maintained in the whole channel if an increase of Re is accompanied by an appropriate increase of Ra_p. The second effect in play involves variations of α; its increase results in the formation of a different boundary layer at the lower wall and a conduction zone above it. An increase of both Re and α reduces the spatial flow modulations and eliminates the spatial parametric resonance. As a result, the secondary motion is driven by the RB effect and all of the critical curves approach a similar asymptote for $Re \to \infty$, as illustrated in figure 13(*a*); the asymptote has been determined numerically. On the other hand, variations of β_{cr} always show a strong dependence on α, as illustrated in figure 13(*b*); this variability does not disappear even in the limit of $Re \to \infty$. The results displayed in figure 14 demonstrate the existence of different β_{cr} for different α even when $Re = 10^5$.

3.3.4. *Longitudinal rolls*

We shall now turn our attention to the longitudinal rolls. Such rolls are parallel to the primary rolls and thus they are orthogonal to the direction of the forced flow (see figure 15). These rolls correspond to the orthogonal rolls in the case of uniform heating. Figure 16 displays variations of the critical conditions as a function of α. It can be seen that the rolls are stationary for $Re = 0$ but begin to be pushed downstream when forced convection is introduced (figure 16*b*). The speed of the downstream movement increases with Re for the complete range of α studied. There is a finite range of α bounded from below, which can lead to the formation of such rolls when $Re = 0$ (figure 16*a*). An increase of Re expands this range towards smaller αs. The minimum of $Ra_{p,cr}$ occurs for $Re \approx 5$ and further increase of Re stabilizes the flow, at least in the range of α studied. There is an interesting evolution of the disturbance pattern at the onset, as illustrated in figure 16(*b*). In the case of natural convection ($Re = 0$) and for $\alpha < 4.2$, the disturbance wavenumber is locked in with the

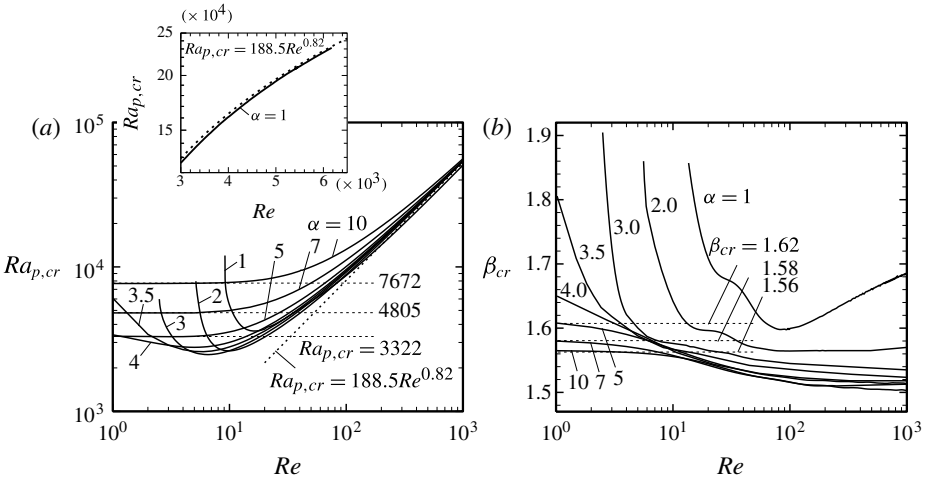

FIGURE 13. The onset conditions required for the formation of the secondary convection in the form of transverse rolls in the fluid flowing through a channel subject to periodic heating of different wavelength (see § 3.3.3): variations of (*a*) the critical Rayleigh number $Ra_{p,cr}$ and (*b*) the critical wavenumber β_{cr} as functions of the Reynolds number Re. The asymptote for large Re is marked in panel (*a*) using the dashed line. No asymptote has been identified in panel (*b*) (see figure 14 for further explanations).

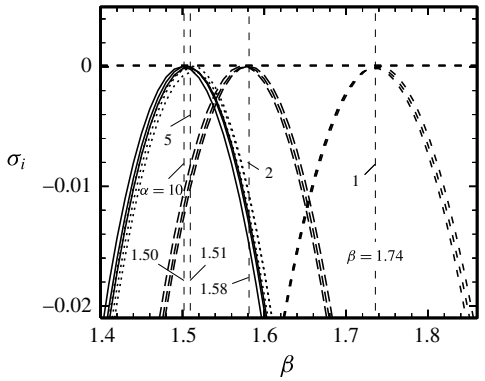

FIGURE 14. Demonstration that an α-independent asymptote for β_{cr} for large Re does not exist. This figure displays variations of the amplification rate σ_i as a function of the wavenumber β of transverse rolls resulting from the application of heating with wavenumbers $\alpha = 1$, 2, 5 and 10 for three values of the Reynolds number, i.e. $Re = 10^4$, 5×10^4 and 10^5. Heating with the Rayleigh number corresponding to the critical conditions for each combination of α and Re has been used. It can be seen that an increase of Re results in $\beta_{cr} \to 1.74$, 1.58, 1.51 and 1.50 for $\alpha = 1$, 2, 5 and 10.

wavenumber of the primary convection according to the relation $\delta_{cr} = \alpha/2$ (figure 16*b*). Heating with larger α generates rolls with δ_{cr} exhibiting a rather complex dependence on α and with the limit point of $\delta_{cr} \to 1.56$ for $\alpha \to \infty$ (Hossain & Floryan 2013*b*). A small increase of Re up to $Re = 5$ maintains a similar structure of variations of δ_{cr} but with the lock-in point moved towards smaller α and the limit point for $\alpha \to \infty$

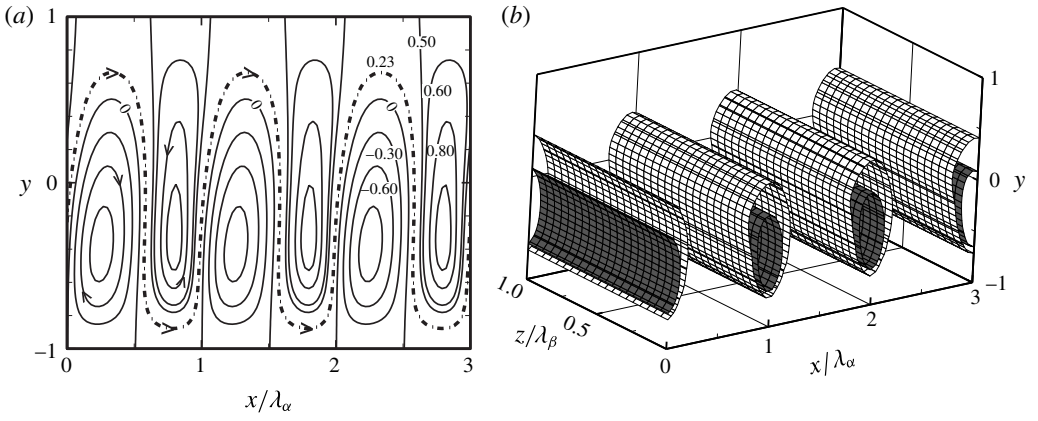

FIGURE 15. The flow structures associated with (*a*) the primary convection and (*b*) the secondary convection in the form of longitudinal rolls at the onset in a flow with $Re = 1$. (*a*) The stream function normalized with its maximum; (*b*) the second invariant of the velocity gradient tensor (see (3.21)). The heating has the wavenumber $\alpha = 3.6$, requires an intensity corresponding to $Ra_{p,cr} = 3191$ and generates the secondary convection with wavenumber $\delta_{cr} = 1.8$ (the lock-in conditions). The rolls are pushed downstream with the phase speed corresponding to $\sigma_r = 0.0015$. This speed increases with an increase of Re.

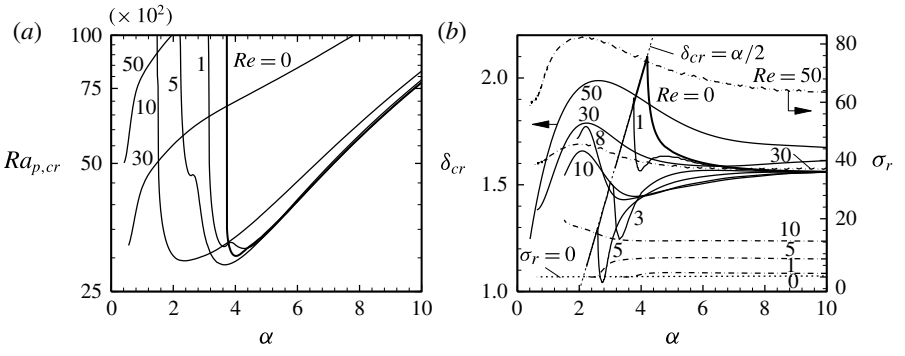

FIGURE 16. The onset conditions required for the formation of the secondary convection in the form of longitudinal rolls in a fluid driven through a periodically heated channel at different Reynolds numbers Re (see § 3.3.4). (*a*) Variations of the critical Rayleigh number Ra_{cr} as a function of the heating wavenumber α. The thick solid line identifies the reference state of $Re = 0$. (*b*) Variations of the critical wavenumber δ_{cr} (solid lines) as a function of the heating wavenumber α, with the thick solid line corresponding to the reference state of $Re = 0$. Also shown are variations of the critical frequency σ_{cr} as a function of the heating wavenumber α (dashed lines). The reference state of $Re = 0$ is marked using the dotted line ($\sigma_{cr} = 0$).

slightly increasing (figure 16*b*). A further increase of Re completely eliminates the lock-in phenomenon and leads to an increase of δ_{cr} for $\alpha < 4.2$. This is due to the elimination of the separation bubbles and thus elimination of the spatial parametric resonance, as has already been discussed in the previous section. At the same time, the limit of δ_{cr} for $\alpha \to \infty$ increases above the reference value of 1.56 found in the case of natural convection.

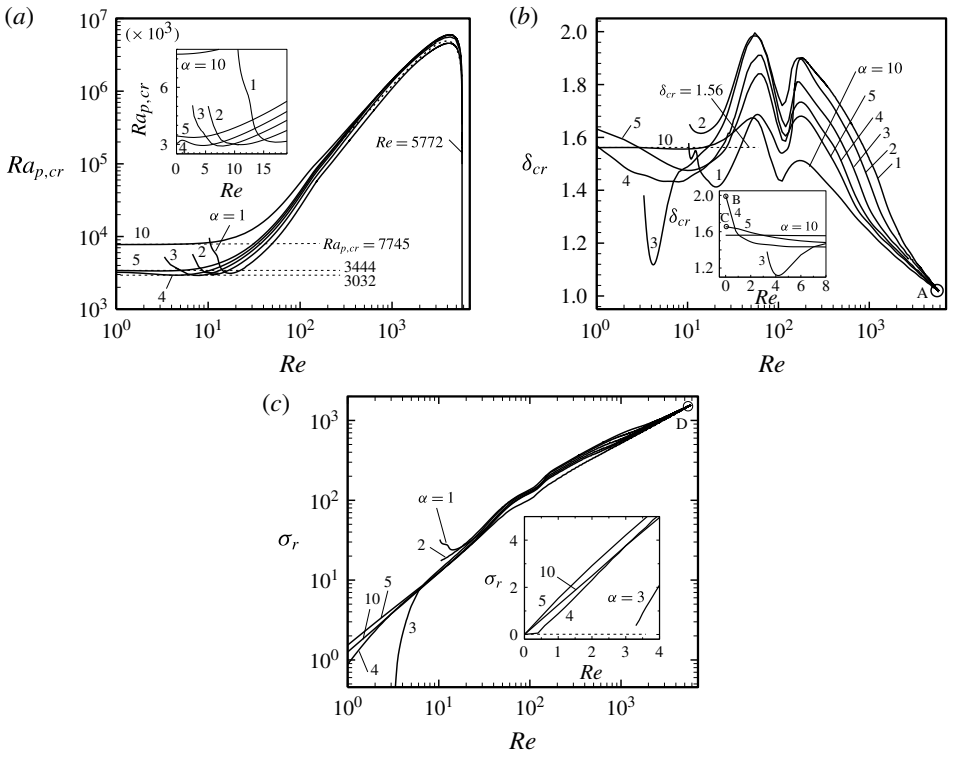

FIGURE 17. The onset conditions required for the formation of the secondary convection in the form of longitudinal rolls in a fluid driven through a channel subject to periodic heating of different wavelength (see § 3.3.4). (*a*) Variations of the critical Rayleigh number $Ra_{p,cr}$, (*b*) variations of the critical wavenumber δ_{cr} and (*c*) variations of the critical frequency σ_r as functions of the Reynolds number Re. Correlation $Ra_{p,cr} = \alpha^{0.2}(61.1Re^{1.386} - 7.2 \times 10^{-7}Re^{3.48})$ valid for $250 < Re < 5772$ is marked in panel (*a*) using the dotted line. The limit points A, B and C in panel (*b*) are located at $(Re, \delta_{cr}) = (5772, 1.02)$, $(0, 2)$ and $(0, 1.66)$, respectively, and the limit point D in panel (*d*) is located at $(Re, \sigma_r) = (5772, 1554)$.

Figure 17 illustrates more explicitly the variations of the critical conditions as a function of Re. The results displayed in figure 17(*a*) demonstrate a complex dependence of $Ra_{p,cr}$ on Re. For small Re ($Re < 5$), $Ra_{p,cr}$ either does not depend on Re or decreases with Re depending on α. Increase of Re above $Re = 5$ results in an increase of $Ra_{p,cr}$ for all α considered. All critical curves exhibit a similar form for $Re > 250$, which leads to a correlation of the form $Ra_{p,cr} = \alpha^{0.2}(61.1\,Re^{1.386} - 7.2 \times 10^{-7}\,Re^{3.48})$. When Re approaches the limiting value of 5772, $Ra_{p,cr}$ rapidly drops off for all α as the instability becomes dominated by shear, similar to the case of uniform heating (§ 3.3.2). The variations of δ_{cr} displayed in figure 17(*b*) underline the complexity of the dependence of the critical conditions on Re. There is a wide range of variations of δ_{cr} as a function of Re for $Re < 5$, dependent on the heating wavenumber. This is followed by rapid but qualitatively similar variations of δ_{cr} for all α for Re between 5 and 250, and different but also qualitatively similar variations for $Re > 250$ with the critical curves approaching the same limit point $(\delta_{cr}, Re) = (1.02, 5772)$ for all α. Figure 17(*c*) illustrates the

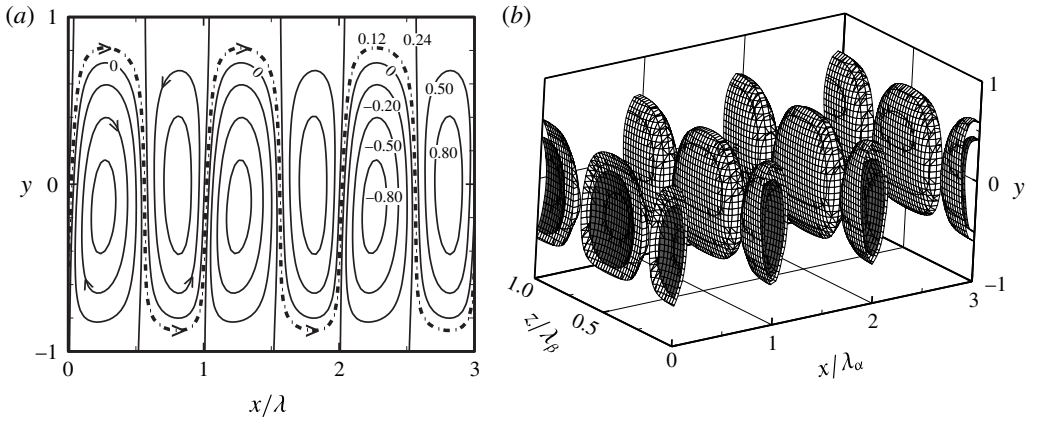

FIGURE 18. The flow structures associated with (*a*) the primary convection and (*b*) the secondary convection in the form of oblique rolls at the onset in a flow with $Re = 1$. (*a*) The stream function normalized by its maximum; (*b*) the second invariant of the velocity gradient tensor (see (3.21)). The heating has the wavenumber $\alpha = 2.5$, requires an intensity corresponding to $Ra_{p,cr} = 2513$ and generates the secondary convection with wavenumbers $\delta_{cr} = 1.25$ and $\beta_{cr} = 0.77$.

evolution of the complex frequency from $\sigma_r = 0$ at $Re = 0$ to $\sigma_r = 1554$ at $Re = 5772$. These changes illustrate morphing of the stationary longitudinal rolls at $Re = 0$ into travelling waves driven by shear for $Re > 5772$.

3.3.5. *Oblique rolls*

The previous two sections discussed the properties of two special classes of rolls, i.e. longitudinal and transverse rolls. The instability can generate rolls with any orientation, i.e. oblique rolls (see figure 18). Figure 19 displays variations of $Ra_{p,cr}$ as a function of roll orientation for $\alpha = 3.5$ for $Re = 0$, 1 and 10. The obliqueness angle χ used in this figure is defined as $\tan(\chi) = \beta/\delta$ and thus $\chi = 0°$ corresponds to longitudinal rolls and $\chi = 90°$ to transverse rolls. Results of this type permit identification of the roll orientation at the onset and variations of the critical roll orientation as a function of Re and α. In the case of this particular heating wavenumber, the oblique rolls play the critical role at $Re = 0$ and $Re = 1$, to be replaced by the transverse rolls at $Re = 10$. Figure 20 displays the critical curves that identify both the critical roll orientation and the corresponding $Ra_{p,cr}$ as a function of Re and α. This figure is limited only to those conditions where the oblique rolls play the critical role. The limit points where either longitudinal or transverse rolls become critical are marked with a black dot.

In all the cases considered, the critical oblique rolls are stationary, i.e. $\sigma_r = 0$. The critical wavevector has x component locked in with the wavevector of the primary instability according to the relation $\delta_{cr} = \alpha/2$, which is a characteristic feature of the spatial resonance (figure 20*b*), while variations of the z component do not follow any regular path. The appearance of the z component results in the three-dimensionalization of the disturbance velocity field, which is another characteristic feature of the spatial resonance (Manor, Hagberg & Meron 2008, 2009). An increase of Re results in the transfer of the limit points towards smaller α; an increase of Re from $Re = 0$ to $Re = 3$ results in the reduction of $Ra_{p,cr}$, which

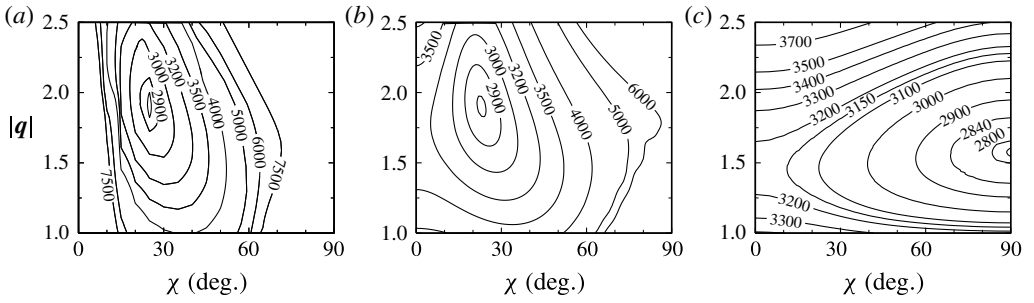

FIGURE 19. The onset conditions required for the formation of the secondary convection in the form of oblique rolls in a fluid driven through a periodically heated channel (see § 3.3.5). (*a–c*) Variations of the critical Rayleigh number $Ra_{p,cr}$ as a function of the magnitude of the disturbance wavevector $|\boldsymbol{q}| = \sqrt{\delta^2 + \beta^2}$ and its orientation angle χ, defined as $\tan(\chi) = \beta/\delta$, for the heating with the wavenumber $\alpha = 3.5$ for the flow Reynolds number $Re = 0$ (*a*), 1 (*b*) and 10 (*c*), respectively.

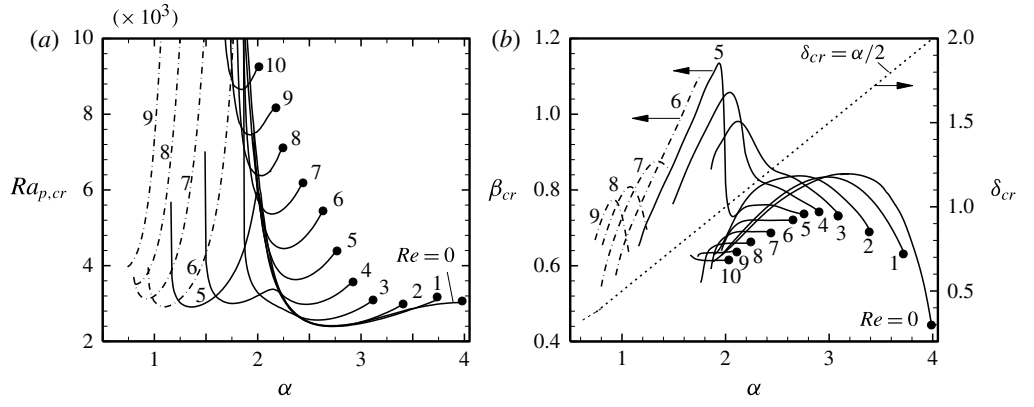

FIGURE 20. The onset conditions required for the formation of the secondary convection in the form of oblique rolls in a fluid driven through a periodically heated channel (see § 3.3.5). Variations of (*a*) the critical Rayleigh number $Ra_{p,cr}$ and (*b*) the critical wavenumbers δ_{cr} and β_{cr} as functions of the heating wavenumber α. The critical curves for $Re > 6$ consist of two segments with the dash-dotted lines used to identify the left segment. Symbols (●) identify the limit points on the α axis where the oblique rolls cease to play the critical role.

can be achieved at any α (see figure 20*a*), but a further increase of Re leads to an increase of $Ra_{p,cr}$. The flow stabilization, which is due to an increase of Re and, at the same time, due to the reduction of α, is consistent with the weakening of the parametric resonance mechanism. It has already been pointed out in the previous two sections that an increase of Re reduces the strength of the separation bubbles, which leads to the reduction of the magnitude of the spatial flow modulation, and this results in the reduction of the strength of the spatial resonance.

The special feature of the oblique rolls is the division of the critical curves into two segments for $Re > 5$. As Re increases above $Re = 3$, the instability expands into smaller α, with the critical curve acquiring two minima (see curve for $Re = 4$ in figure 20*a*). A further increase of Re amplifies this division (see curve for $Re = 5$ in figure 20*a*) and

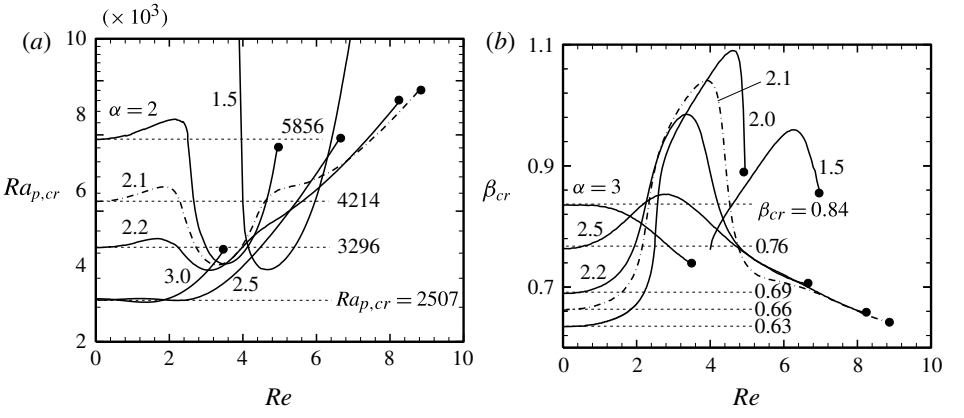

FIGURE 21. The onset conditions required for the formation of the secondary convection in the form of oblique rolls in a fluid driven through a periodically heated channel (see § 3.3.5). Variations of (*a*) the critical Rayleigh number $Ra_{p,cr}$ and (*b*) the critical wavenumber β_{cr} as functions of the Reynolds number Re. Symbols (●) identify the limit points on the Re axis where the oblique rolls cease to play the critical role. Note that $\delta_{cr} = \alpha/2$ for oblique rolls.

leads to separation of the critical curves into two segments (see curves for $Re = 6$–10 in figure 20*a*). These segments might join each other at much higher Ra_p, but this question has not been investigated. The formation of the left segment of the critical curve, which extends into α values much smaller than those found for $Re = 0$, suggests that another instability mechanism may contribute to the system dynamics. In this case the primary convection has the form of very elongated rolls (Hossain & Floryan 2013*a*), the spatial resonance remains active (see the form of the critical wavevector in figure 20*b*) and so the most likely mechanism is the reinvigorated RB mechanism. This question has not been pursued any further in this study.

The role of Re in the onset of oblique rolls is illustrated in figure 21. These rolls play the critical role for very small Re and undergo a very rapid α-dependent transformation due to small changes of Re. Generally, they cease to play the critical role for $Re < 10$, but these conditions vary greatly with α.

3.3.6. *The critical conditions*

The final question to be discussed is the identification of the type of rolls that is generated at the onset, i.e. discussion of the competition between different rolls and the identification of patterns of motion that result from the instability. The discussion presented in the previous sections demonstrates a rapid change in the instability patterns for small Re, with the transverse rolls eventually winning the competition. This process is illustrated in figure 22. When $Re = 0$, the oblique rolls dominate for $\alpha < 4.03$, the longitudinal rolls dominate for $4.03 < \alpha < 4.46$ and the transverse rolls dominate for $\alpha > 4.46$. At $Re = 1$ the changeover points are at $\alpha = 3.77$ and $\alpha = 4.34$. The longitudinal rolls cease to play the critical role at $Re = 2$ and the changeover between the oblique and transverse rolls occurs at $\alpha = 3.68$. The changeover point moves to $\alpha = 3.16$, 2.77, 2.38, 1.72 and 1.2 for $Re = 3$, 4, 5, 6 and 8, respectively. The transverse rolls dominate at $Re = 10$. These predictions are correct assuming that there are no additional effects that may provide a preference for certain type of rolls.

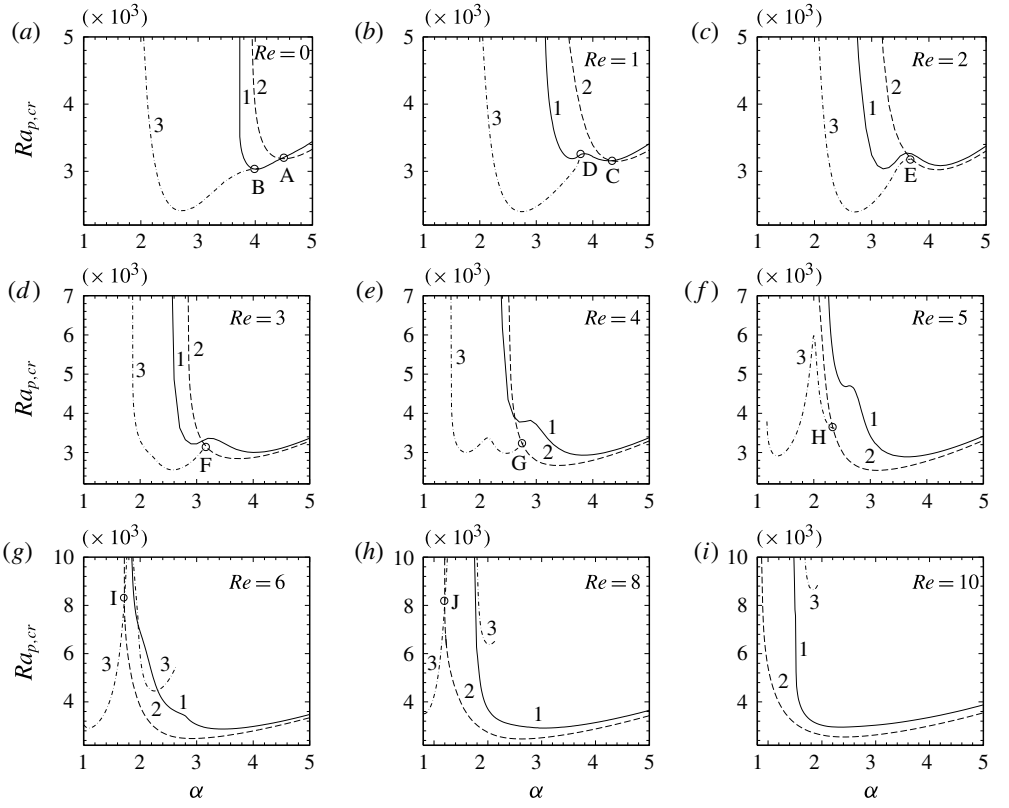

FIGURE 22. The onset conditions for the secondary convection (see § 3.3.6). (*a–i*) Variations of the critical conditions for the transverse, longitudinal and oblique rolls as a function of the heating wavenumber α for the flow Reynolds number $Re = 0$, 1, 2, 3, 4, 5, 6, 8 and 10, respectively. Labels 1, 2 and 3 identify the longitudinal, transverse and oblique rolls, respectively. Points A, B, C, D, E, F, G, H, I and J have coordinates $(\alpha, Ra_{p,cr}) = (4.46, 3192)$, $(4.03, 3032)$, $(4.34, 3156)$, $(3.77, 3201)$, $(3.68, 3178)$, $(3.16, 3162)$, $(2.77, 3251)$, $(2.38, 3623)$, $(1.72, 8234)$ and $(1.2, 8040)$, respectively.

3.4. *Transition to secondary states with heating applied at the upper wall*

It can be shown that the transformation discussed in § 2.4 applies also to the analysis of stability of the primary convection. As a result, the transition to secondary states occurs under the same conditions as in the case of heating applied at the lower wall, while the disturbance flow patterns exhibit phase differences similar to those discussed by Hossain & Floryan (2014).

4. Summary

Mixed convection in a channel exposed to heating that is periodic in the flow direction has been analysed. The heating can be applied either at the lower or at the upper wall and results in a sinusoidal wall temperature distribution characterized by the wavenumber α and the amplitude expressed in terms of the Rayleigh number Ra_p. The primary convection represents a forced response to the applied heating and has the form of counter-rotating rolls whose pattern is dictated by the pattern of the heating. This convection occurs regardless of the magnitude of the heating. Detailed results have been presented for fluids with Prandtl number $Pr = 0.71$.

The largest heat transfer across the channel occurs for the natural convection ($Re = 0$) and diminishes with an increase of the forced flow component (increase of Re). The most effective heating wavenumber is $\alpha \approx 1$, with the heat transfer rapidly decreasing for smaller and larger α. The magnitude of the heat transfer is proportional to Ra_p for small enough heating intensity but its growth saturates for $Ra_p = O(10^3)$. Heating with large α leads to the formation of a boundary layer adjacent to the heated wall and formation of a conduction zone in the remaining part of the channel where the temperature varies only in the vertical direction.

The primary convection with large enough Ra_p undergoes transition to a secondary convection, which changes the heat transfer process in a qualitative sense. This transition is driven by a mix of the RB mechanism, which dominates for large α, with the spatial parametric resonance, which dominates for $\alpha = O(1)$. The critical conditions have been determined for the range of α and Re of practical interest. Three types of rolls can be formed at the onset, i.e. longitudinal, transverse and oblique rolls, depending on α and Re. The detailed characteristics of these rolls have been given for the range of Re where the heating determines the onset conditions. The longitudinal rolls are stationary at $Re = 0$ but begin to travel in the downstream direction as Re increases. These rolls undergo morphing into TS waves as Re increases, with transition completed at $Re = 5772$. Wavenumber locking between the primary and secondary convection is observed for small enough Re and α; an increase of Re above $Re = 5$ eliminates the lock-in phenomenon. The transverse rolls remain stationary as Re increases; the corresponding critical Ra_p approaches an asymptote for $\alpha \to \infty$, which can be predicted analytically by taking advantage of knowledge about the formation of the conduction zone away from the heated wall. An increase of Re leads to the formation of another type of boundary layer; the corresponding Ra_p approaches an asymptote as $Re \to \infty$ whose form has been determined numerically. Oblique rolls play a critical role only for small enough Re and small enough α. The character of the instability motion undergoes rapid α-dependent changes for small Re. A sufficient increase of Re results in the dominance of the transverse rolls, assuming that no symmetry-breaking effects are present. The heat transfer properties of the saturation states remain to be determined.

The system response is the same regardless of whether the heating is applied at the lower or at the upper wall.

Acknowledgements

This work has been carried out with the financial support of the Natural Sciences and Engineering Research Council (NSERC) of Canada.

Appendix A

Definitions of functions used in § 2.3:

$$\theta_{00} = \frac{1}{4} - \frac{y}{4}, \tag{A 1}$$

$$\theta_{02} = -\frac{y^3}{24} + \frac{y^2}{8} + \frac{y}{24} - \frac{1}{8}, \tag{A 2}$$

$$\theta_{04} = -\frac{y^5}{480} + \frac{y^4}{96} + \frac{y^3}{144} - \frac{y^2}{16} - \frac{7y}{1440} + \frac{5}{96}, \tag{A 3}$$

$$F_{U1}(y) = \frac{y^4}{96} - \frac{y^3}{24} - \frac{y^2}{80} + \frac{y}{24} + \frac{1}{480}, \tag{A 4}$$

$$F_{V2}(y) = -\frac{y^5}{480} + \frac{y^4}{96} + \frac{y^3}{240} - \frac{y^2}{48} - \frac{y}{480} + \frac{1}{96}, \tag{A 5}$$

$$F_{P0}(y) = -\frac{y^2}{8} + \frac{y}{4} + \frac{1}{40}, \tag{A 6}$$

$$F_{\Theta 1} = -\frac{y^5}{48} + \frac{y^4}{48} + \frac{y^3}{24} - \frac{y^2}{8} - \frac{7y}{240} + \frac{5}{48}, \tag{A 7}$$

$$\begin{aligned} F_{U21}(y) &= -\frac{y^8}{26\,880} + \frac{y^7}{10\,080} + \frac{y^6}{2880} - \frac{y^5}{480} - \frac{7y^4}{1152} + \frac{5y^3}{288} \\ &\quad + \frac{107y^2}{100\,800} - \frac{31y}{2016} - \frac{1}{6400}, \end{aligned} \tag{A 8}$$

$$\begin{aligned} F_{U22}(y) &= -\frac{y^8}{8960} + \frac{y^7}{2016} + \frac{7y^6}{14\,400} - \frac{y^5}{480} - \frac{y^4}{1152} + \frac{y^3}{288} \\ &\quad + \frac{19y^2}{33\,600} - \frac{19y}{10\,080} - \frac{29}{403\,200}, \end{aligned} \tag{A 9}$$

$$\begin{aligned} F_{V31}(y) &= -\frac{y^9}{241\,920} + \frac{y^8}{80\,640} + \frac{y^7}{20\,160} - \frac{y^6}{2880} - \frac{7y^5}{28\,800} \\ &\quad + \frac{5y^4}{1152} + \frac{107y^3}{302\,400} - \frac{31y^2}{4032} - \frac{y}{6400} + \frac{33}{8960}, \end{aligned} \tag{A 10}$$

$$\begin{aligned} F_{V32}(y) &= -\frac{y^9}{80\,640} + \frac{y^8}{16\,128} + \frac{y^7}{14\,400} - \frac{y^6}{2880} - \frac{y^5}{5760} + \frac{y^4}{1152} \\ &\quad + \frac{19y^3}{100\,800} - \frac{19y^2}{20\,160} - \frac{29y}{403\,200} + \frac{29}{80\,640}, \end{aligned} \tag{A 11}$$

$$F_{P1} = -\frac{y^6}{480} + \frac{y^5}{240} + \frac{y^4}{96} - \frac{y^3}{24} - \frac{7y^2}{480} + \frac{5y}{48} + \frac{107}{50\,400}, \tag{A 12}$$

$$\begin{aligned} F_{\Theta 21} &= \frac{y^7}{26\,880} - \frac{y^6}{3840} + \frac{y^5}{6400} + \frac{y^4}{1280} - \frac{y^3}{1280} \\ &\quad - \frac{y^2}{1280} + \frac{79y}{134\,400} + \frac{1}{3840}, \end{aligned} \tag{A 13}$$

$$\begin{aligned} F_{\Theta 22} &= \frac{1}{201\,600}\,(\,35y^9 - 75y^8 - 260y^7 + 980y^6 + 714y^5 - 3850y^4 \\ &\quad - 980y^3 + 10\,500y^2 + 491y - 7555\,), \end{aligned} \tag{A 14}$$

$$\begin{aligned} F_{\Theta 23} &= -\frac{y^7}{40\,320} + \frac{y^6}{5760} - \frac{y^5}{4800} - \frac{y^4}{2880} + \frac{y^3}{1152} - \frac{y^2}{1920} \\ &\quad - \frac{y}{1575} + \frac{1}{1440}, \end{aligned} \tag{A 15}$$

$$F_{U31}(y) = \frac{y^6}{960} - \frac{y^5}{160} - \frac{11y^4}{2880} + \frac{5y^3}{144} + \frac{109y^2}{33\,600} - \frac{41y}{1440} - \frac{47}{100\,800}, \tag{A 16}$$

$$\begin{aligned} F_{U32}(y) &= -\frac{y^{12}}{4561\,920} + \frac{y^{11}}{1478\,400} + \frac{23y^{10}}{7257\,600} - \frac{y^9}{48\,384} - \frac{31y^8}{1612\,800} \\ &\quad + \frac{31y^7}{120\,960} + \frac{949y^6}{18\,144\,000} - \frac{y^5}{1152} - \frac{73y^4}{967\,680} \\ &\quad + \frac{323y^3}{241\,920} + \frac{181\,171y^2}{4036\,032\,000} - \frac{1337y}{1900\,800} - \frac{398\,309}{72\,648\,576\,000}, \end{aligned} \tag{A 17}$$

$$F_{U33}(y) = -\frac{y^{12}}{1520\,640} + \frac{y^{11}}{295\,680} + \frac{37y^{10}}{7257\,600} - \frac{19y^9}{725\,760} - \frac{29y^8}{1612\,800} + \frac{11y^7}{120\,960} + \frac{71y^6}{2016\,000} - \frac{y^5}{5760} - \frac{199y^4}{4838\,400} + \frac{47y^3}{241\,920} + \frac{323y^2}{14\,676\,480} - \frac{709y}{7983\,360} - \frac{185\,711}{72\,648\,576\,000}, \tag{A 18}$$

$$F_{U34}(y) = -\frac{y^{12}}{7603\,200} + \frac{y^{11}}{2661\,120} + \frac{13y^{10}}{7257\,600} - \frac{y^9}{103\,680} - \frac{17y^8}{1612\,800} + \frac{11y^7}{120\,960} + \frac{7y^6}{172\,800} - \frac{y^5}{1152} - \frac{491y^4}{4838\,400} + \frac{1511y^3}{241\,920} + \frac{15\,661y^2}{192\,192\,000} - \frac{8717y}{1596\,672} - \frac{120\,749}{10\,378\,368\,000}, \tag{A 19}$$

$$F_{U35}(y) = \frac{y^{10}}{14\,515\,200} - \frac{y^9}{1451\,520} + \frac{y^8}{806\,400} + \frac{y^7}{302\,400} - \frac{y^6}{69\,120} + \frac{y^5}{57\,600} + \frac{y^4}{18\,900} - \frac{y^3}{4320} - \frac{197y^2}{4224\,000} + \frac{307y}{1451\,520} + \frac{2749}{399\,168\,000}, \tag{A 20}$$

$$F_{U36}(y) = \frac{y^{10}}{8294\,400} - \frac{y^9}{829\,440} + \frac{23y^8}{6451\,200} + \frac{y^7}{483\,840} - \frac{49y^6}{6912\,000} + \frac{y^5}{230\,400} - \frac{y^4}{55\,296} - \frac{y^3}{69\,120} + \frac{1021y^2}{39\,424\,000} + \frac{269y}{29\,030\,400} - \frac{14\,083}{3193\,344\,000}, \tag{A 21}$$

$$F_{V41}(y) = -\frac{y^7}{6720} + \frac{y^6}{960} + \frac{11y^5}{14\,400} - \frac{5y^4}{576} - \frac{109y^3}{100\,800} + \frac{41y^2}{2880} + \frac{47y}{100\,800} - \frac{19}{2880}, \tag{A 22}$$

$$F_{V42}(y) = \frac{y^{13}}{59\,304\,960} - \frac{y^{12}}{17\,740\,800} - \frac{23y^{11}}{79\,833\,600} + \frac{y^{10}}{483\,840} + \frac{31y^9}{14\,515\,200} - \frac{31y^8}{967\,680} - \frac{949y^7}{127\,008\,000} + \frac{y^6}{6912} + \frac{73y^5}{4838\,400} - \frac{323y^4}{967\,680} - \frac{181\,171y^3}{12\,108\,096\,000} + \frac{1337y^2}{3\,801\,600} + \frac{398\,309y}{72\,648\,576\,000} - \frac{1411}{10\,644\,480}, \tag{A 23}$$

$$F_{V43}(y) = \frac{y^{13}}{19\,768\,320} - \frac{y^{12}}{3548\,160} - \frac{37y^{11}}{79\,833\,600} + \frac{19y^{10}}{7257\,600} + \frac{29y^9}{14\,515\,200} - \frac{11y^8}{967\,680} - \frac{71y^7}{14\,112\,000} + \frac{y^6}{34\,560} + \frac{199y^5}{24\,192\,000} - \frac{47y^4}{967\,680} - \frac{323y^3}{44\,029\,440} + \frac{709y^2}{15\,966\,720} + \frac{185\,711y}{72\,648\,576\,000} - \frac{359}{22\,809\,600}, \tag{A 24}$$

$$F_{V44}(y) = \frac{y^{13}}{98\,841\,600} - \frac{y^{12}}{31\,933\,440} - \frac{13y^{11}}{79\,833\,600} + \frac{y^{10}}{1036\,800} + \frac{17y^9}{14\,515\,200} - \frac{11y^8}{967\,680} - \frac{y^7}{172\,800} + \frac{y^6}{6912} + \frac{491y^5}{24\,192\,000} - \frac{1511y^4}{967\,680} - \frac{15\,661y^3}{576\,576\,000} + \frac{8717y^2}{3193\,344} + \frac{120\,749y}{10\,378\,368\,000} - \frac{69\,323}{53\,222\,400}, \tag{A 25}$$

$$F_{V45}(y) = -\frac{y^{11}}{79\,833\,600} + \frac{y^{10}}{7257\,600} - \frac{y^9}{3628\,800} - \frac{y^8}{1209\,600} + \frac{y^7}{241\,920} - \frac{y^6}{172\,800} - \frac{y^5}{47\,250} + \frac{y^4}{8640} + \frac{197y^3}{6336\,000} - \frac{307y^2}{1451\,520} - \frac{2749y}{199\,584\,000} + \frac{53}{518\,400}, \tag{A 26}$$

$$F_{V46}(y) = -\frac{y^{11}}{45\,619\,200} + \frac{y^{10}}{4147\,200} - \frac{23y^9}{29\,030\,400} - \frac{y^8}{1935\,360} + \frac{7y^7}{3456\,000} - \frac{y^6}{691\,200} + \frac{y^5}{138\,240} + \frac{y^4}{138\,240} - \frac{1021y^3}{59\,136\,000} - \frac{269y^2}{29\,030\,400} + \frac{14\,083y}{1596\,672\,000} + \frac{109}{29\,030\,400}, \tag{A 27}$$

$$F_{\Theta 31}(y) = -\frac{y^7}{1008} + \frac{y^6}{240} + \frac{y^5}{60} - \frac{y^4}{24} - \frac{7y^3}{144} + \frac{3y^2}{16} + \frac{83y}{2520} - \frac{3}{20}, \tag{A 28}$$

$$F_{\Theta 32}(y) = \frac{y^{13}}{898\,560} - \frac{y^{12}}{354\,816} - \frac{59y^{11}}{4435\,200} + \frac{211y^{10}}{3628\,800} + \frac{487y^9}{7257\,600} - \frac{23y^8}{53\,760} - \frac{121y^7}{604\,800} + \frac{41y^6}{17\,280} + \frac{1471y^5}{4032\,000} - \frac{3611y^4}{483\,840} - \frac{491y^3}{1209\,600} + \frac{1511y^2}{80\,640} + \frac{966\,443y}{5189\,184\,000} - \frac{1059\,757}{79\,833\,600}, \tag{A 29}$$

$$F_{\Theta 33}(y) = \frac{y^{11}}{10\,6444\,800} - \frac{y^{10}}{29\,030\,400} - \frac{y^9}{5806\,080} + \frac{y^8}{645\,120} + \frac{y^7}{691\,200} - \frac{y^6}{27\,648} - \frac{107y^5}{24\,192\,000} + \frac{31y^4}{193\,536} + \frac{y^3}{153\,600} - \frac{33y^2}{71\,680} - \frac{769y}{228\,096\,000} + \frac{9721}{29\,030\,400}, \tag{A 30}$$

$$F_{\Theta 34}(y) = \frac{y^{11}}{35\,481\,600} - \frac{y^{10}}{5806\,080} - \frac{y^9}{4147\,200} + \frac{y^8}{645\,120} + \frac{y^7}{967\,680} - \frac{y^6}{138\,240} - \frac{19y^5}{8064\,000} + \frac{19y^4}{967\,680} + \frac{29y^3}{9676\,800} - \frac{29y^2}{645\,120} - \frac{2333y}{1596\,672\,000} + \frac{181}{5806\,080}, \tag{A 31}$$

$$F_{\Theta 35}(y) = -\frac{y^{11}}{2027\,520} + \frac{23y^{10}}{6451\,200} - \frac{3y^9}{716\,800} - \frac{y^8}{36\,864} + \frac{47y^7}{645\,120} + \frac{37y^6}{460\,800} - \frac{259y^5}{768\,000} + \frac{163y^4}{9676\,800} + \frac{13\,033y^3}{19\,353\,600} - \frac{217y^2}{307\,200} - \frac{430\,411y}{1064\,448\,000} + \frac{12\,247}{19\,353\,600}, \tag{A 32}$$

$$F_{\Theta 36}(y) = -\frac{y^{11}}{7884\,800} + \frac{7y^{10}}{8294\,400} - \frac{y^9}{58\,060\,800} - \frac{37y^8}{6451\,200} + \frac{y^7}{276\,480} + \frac{y^6}{55\,296} - \frac{293y^5}{16\,128\,000} - \frac{247y^4}{9676\,800} + \frac{731y^3}{19\,353\,600} + \frac{29y^2}{6451\,200} - \frac{73\,691y}{3193\,344\,000} + \frac{13}{1658\,880}. \tag{A 33}$$

REFERENCES

AHLERS, G., GROSSMANN, S. & LOHSE, D. 2009 Heat transfer and large scale dynamics in turbulent Rayleigh–Bénard convection. *Rev. Mod. Phys.* **81**, 503–537.

BELTRAME, P., KNOBLOCH, E., HÄNGGI, P. & THIELE, U. 2011 Rayleigh and depinning instabilities of forced liquid ridges on heterogeneous substrates. *Phys. Rev.* E **83**, 016305.

BÉNARD, H. 1900 Les tourbillons cellulaires dans une nappe liquide. *Rev. Gén. Sci. Pure Appl.* **11**, 1261–1271.

BLOCH, F. 1928 Über die Quantenmechanik der Elektronen in Kristallgittern. *Z. Phys.* **52**, 555–600.

BODENSCHATZ, E., PESCH, W. & AHLERS, G. 2000 Recent developments in Rayleigh–Bénard convection. *Annu. Rev. Fluid Mech.* **32**, 709–778.

CHILLA, F. & SCHUMACHER, J. 2012 New perspectives in turbulent Rayleigh–Bénard convection. *Eur. Phys. J.* E **35**, 58–82.

CLEVER, R. M. & BUSSE, F. H. 1991 Instabilities of longitudinal rolls in the presence of Poiseuille flow. *J. Fluid Mech.* **229**, 529–617.

CODDINGTON, E. A. & LEVINSON, N. 1965 *Theory of Ordinary Differential Equations*. McGraw-Hill.

DUBIEF, Y. & DELCAYRE, F. 2000 On coherent-vortex identification in turbulence. *J. Turbul.* **1**, 011.

FLORYAN, J. M. 1997 Stability of wall bounded shear layers in the presence of simulated distributed surface roughness. *J. Fluid Mech.* **335**, 29–55.

FLORYAN, J. M. 2003 Vortex instability in a diverging–converging channel. *J. Fluid Mech.* **482**, 17–50.

FLORYAN, J. M. 2012 The thermo-superhydrophobic effect. *Bull. Am. Phys. Soc.* **57** (1), X50.00015.

FREUND, G., PESCH, W. & ZIMMERMANN, W. 2011 Rayleigh–Bénard convection in the presence of spatial temperature modulations. *J. Fluid Mech.* **673**, 318–348.

GAGE, K. S. & REID, W. H. 1968 The stability of thermally stratified plane Poiseuille flow. *J. Fluid Mech.* **33**, 21–32.

HASNAOUI, M., RILGEN, E., VASSEUR, P. & ROBILLARD, L. 1991 Mixed convective heat transfer in a horizontal channel heated periodically from below. *Numer. Heat Transfer* A **20**, 297–315.

HOSSAIN, M. Z. & FLORYAN, J. M. 2013*a* Heat transfer due to natural convection in a periodically heated slot. *Trans. ASME: J. Heat Transfer* **135**, 022503.

HOSSAIN, M. Z. & FLORYAN, J. M. 2013*b* Instabilities of natural convection in a periodically heated layer. *J. Fluid Mech.* **733**, 33–67.

HOSSAIN, M. Z. & FLORYAN, J. M. 2014 Natural convection in a fluid layer periodically heated from above. *Phys. Rev.* E **90**, 023015.

HOSSAIN, M. Z., FLORYAN, D. & FLORYAN, J. M. 2012 Drag reduction due to spatial thermal modulations. *J. Fluid Mech.* **713**, 398–419.

HOWARD, L. N. & KRISHNAMURTI, R. 1986 Large-scale flow in turbulent convection: a mathematical model. *J. Fluid Mech.* **170**, 385–410.

HUGHES, G. O. & GRIFFITHS, R. W. 2008 Horizontal convection. *Annu. Rev. Fluid Mech.* **40**, 185–208.

KELLY, R. E. 1994 The onset and development of thermal convection in fully developed shear flows. *Adv. Appl. Mech.* **31**, 35–112.

KELLY, R. E. & PAL, D. 1976*a* Thermal convection induced between non-uniformly heated horizontal surfaces. In *Proceedings of the 1976 Heat Transfer and Fluid Mechanics Institute*, pp. 1–17. Stanford University Press.

KELLY, R. E. & PAL, D. 1976*b* Thermal convection with spatially periodic boundary conditions: resonant wavelength excitation. *J. Fluid Mech.* **86**, 433–456.

KOSCHMIEDER, E. L. 1993 *Bénard Cells and Taylor Vortices*. Cambridge University Press.

KRISHNAN, M., UGAZ, V. M. & BURNS, M. A. 2002 PCR in a Rayleigh–Bénard convection cell. *Science* **298**, 793.

LENARDIC, A., MORESI, L., JELLINEK, A. M. & MANGA, M. 2005 Continental insulation, mantle cooling, and the surface area of oceans and continents. *Earth Planet. Sci. Lett.* **234**, 317–333.

LOHSE, D. & XIA, K.-Q. 2010 Small-scale properties of turbulent Rayleigh–Bénard convection. *Annu. Rev. Fluid Mech.* **42**, 335–364.

MANOR, A., HAGBERG, A. & MERON, E. 2008 Wavenumber locking in spatially forced pattern-forming systems. *Europhys. Lett.* **83**, 10005.

MANOR, R., HAGBERG, A. & MERON, E. 2009 Wavenumber locking and pattern formation in spatially forced systems. *New J. Phys.* **11**, 063016.

MARCQ, S. & WEISS, J. 2012 Influence of sea ice lead-width distribution on turbulent heat transfer between the ocean and the atmosphere. *Cryosphere* **6**, 143–156.

MAXWORTHY, T. 1997 Convection into domains with open boundaries. *Annu. Rev. Fluid Mech.* **29**, 327–371.

PELLEW, A. & SOUTHWELL, R. V. 1940 On maintained convective motion in a fluid heated from below. *Proc. R. Soc. Lond.* A **176**, 312–343.

RAYLEIGH, J. W. S. 1916 On convection currents in a horizontal layer of fluid, when the higher temperature is on the under side. *Phil. Mag.* **32**, 529–546.

RIPESI, P., BIFERALE, L., SBRAGAGLIA, M. & WIRTH, A. 2014 Natural convection with mixed insulating and conducting boundary conditions: low- and high-Rayleigh-number regimes. *J. Fluid Mech.* **742**, 636–663.

SIGGERS, J. H., KERSWELL, R. R. & BALMFORTH, N. J. 2004 Bounds on horizontal convection. *J. Fluid Mech.* **517**, 55–70.

WEISS, S., SEIDEN, G. & BODENSCHATZ, E. 2012 Pattern formation in spatially forced thermal convection. *New J. Phys.* **14**, 053010.

WINTERS, K. B. & YOUNG, W. R. 2009 Available potential energy and buoyancy variance in horizontal convection. *J. Fluid Mech.* **629**, 221–230.